Available on the CERN CDS information server **CMS PAS SUS-11-015**

CMS Physics Analysis Summary

Contact: cms-pag-conveners-susy@cern.ch 2011/09/09

Search for supersymmetry in pp collisions at $\sqrt{s} = 7$ TeV in events with a single lepton, jets, and missing transverse momentum

The CMS Collaboration

Abstract

Preliminary results are reported from a search for physics beyond the standard model in proton-proton collisions at a center-of-mass energy of 7 TeV, focusing on the signature with a single, isolated, high-transverse momentum lepton (electron or muon), energetic jets, and large missing transverse momentum. The data sample comprises an integrated luminosity of 1.1 fb^{-1}, recorded by the CMS experiment at the LHC. The search is motivated by models of new physics, including supersymmetry. Standard model backgrounds are determined from control samples in the data using two complementary methods. The observed yields of events in the signal region are consistent with the background predictions. The results are interpreted in terms of limits on the parameter space for the constrained minimal supersymmetric extension of the standard model.

1 Introduction

Searches for new physics at the TeV energy scale are motivated by several considerations, ranging from the strong astrophysical evidence for dark matter [1–4] to theoretical issues associated with explaining the observed particle masses and their hierarchy [5, 6]. In this paper, we report results from a search for new physics in proton-proton collisions at a center-of-mass energy of 7 TeV, focusing on the signature with a single isolated lepton (electron or muon), multiple energetic jets, and large missing momentum transverse to the beam direction ($\not\!\!E_{\mathrm{T}}$). The data sample was collected by the Compact Muon Solenoid (CMS) experiment during 2011 at the Large Hadron Collider (LHC) and corresponds to an integrated luminosity of 1.1 fb^{-1} [7].

The search signature arises naturally in several theoretical frameworks for new physics, among them supersymmetry (SUSY) [8–13]. SUSY models predict a spectrum of new particles with couplings identical to those of the standard model (SM), but with spins differing by half a unit with respect to their SM partners. In many models, a multiplicatively conserved quantum number, *R* parity, is introduced, constraining SUSY particles to be produced in pairs and SUSY particle decay chains to end with the lightest supersymmetric particle (LSP). In some scenarios, the LSP is a neutralino, a heavy, electrically neutral, weakly interacting particle with the characteristics required of a dark-matter candidate.

Searches at the Tevatron [14–16] and LEP [17–21] have found no evidence as yet for SUSY particles, demonstrating that, if supersymmetry exists, it is broken, with SUSY particle masses typically greater than 100–300 GeV. Recently, searches from the CMS [22–28] and ATLAS [29–33] experiments have extended the sensitivity to higher mass scales. In particular, both CMS [28] and ATLAS [29] have reported constraints on SUSY models based on searches in the single-lepton channel, using data samples with integrated luminosities of about 35 pb^{-1} per experiment.

At the LHC, relatively large cross sections for SUSY particle production (up to tens of pb) can arise from strong-interaction (QCD) processes leading to the production of gluino-gluino, squark-gluino, squark-squark, and squark-antisquark pairs. The search signature reflects the complex decay chains of the heavy, strongly coupled SUSY particles. The isolated lepton indicates a weak decay of a heavy particle, either a W boson or a new particle. Large missing momentum transverse to the beam direction can be carried by a neutrino or, in the case of new physics, by one or more heavy, weakly interacting particles, such as the LSP. Finally, multiple jets can arise from quarks and gluons produced in the decay chains. This signature arises in many SUSY models, including the constrained minimal supersymmetric extension to the standard model (CMSSM) [34, 35], which we use to interpret the results.

The SUSY signal is not characterized by any narrow peaks, but rather by broad distributions that extend to higher values of the kinematic variables than those of the SM backgrounds. These backgrounds arise primarily from the production of $\mathrm{t\bar{t}}$, W+jets, and QCD multijet events. It is therefore critical to determine the extent of the tails of the SM background distributions. We use methods that are primarily based on control samples in the data, sometimes in conjunction with certain reliable information from simulated event samples or from previous measurements.

Two methods are used to probe the event sample. The *Lepton Spectrum method*, was used in the CMS single-lepton [28] and opposite-sign dilepton [25] SUSY searches in the 2010 data. It uses the observed lepton spectrum to predict the $\not\!\!E_{\mathrm{T}}$ spectrum under the null (SM) hypothesis. This measurement is sensitive to SUSY models in which the $\not\!\!E_{\mathrm{T}}$ distribution is decoupled from the lepton spectrum, as is the case when two undetected LSPs produce a large missing transverse momentum. The *Lepton-Projection Variable method* uses the $\mathrm{L_P}$ variable, which was developed for the CMS measurement of the W polarization in W+jets events [36]. This variable, described

in Section 6, is correlated to the helicity angle of the lepton in the W-boson rest frame. The method takes advantage of well understood properties of the W polarization in $\mathrm{t\bar{t}}$ and W+jets events, which are the dominant backgrounds.

Given the large range of potential signal models, the use of two methods for the background determination provides valuable information to ensure that the event sample is understood.

The paper is organized as follows. Sections 2 and 3 describe the CMS detector and the event samples, respectively. The event preselection requirements are discussed in Section 4. Sections 5 and 6 describe the Lepton Spectrum method and the Lepton Projection method, respectively, for obtaining SM background estimates from control samples in the data. The observed yields in the data are compared with the background estimate obtained for each method. Finally, the results, interpretation, and conclusions of the analysis are presented in Sections 7 and 8.

2 CMS Detector

The CMS detector, described in detail in Ref. [37], is a multipurpose apparatus designed to study high-p_{T} physics processes in proton-proton collisions, as well as a broad range of phenomena in heavy-ion collisions. The central element of CMS is a 3.8 T superconducting solenoid, 13 m in length and 6 m in diameter. Within the magnet are (in order of increasing radius from the beam pipe) the high-precision silicon-pixel and silicon-strip detectors for charged particle tracking; a lead tungstate crystal electromagnetic calorimeter for measurements of photons, electrons, and the electromagnetic component of jets; and a hadron calorimeter, constructed from scintillating tiles and brass absorbers, for jet-energy measurements. Beyond the magnet is the muon system, comprising drift-tube, cathode-strip, and resistive-plate detectors interleaved with steel absorbers. Each detector system comprises subsystems that cover the central (barrel) and forward (endcap) regions.

In describing the angular distribution of particles and the acceptance of the detector, we frequently make use of the pseudorapidity, $\eta = -\ln[\tan(\theta/2)]$, where the polar angle θ of the particle's momentum vector is measured with respect to the z axis of the CMS coordinate system. The z axis points along the direction of the counterclockwise rotating beam; the azimuthal angle ϕ is measured in a plane perpendicular to this axis. The separation between two momentum vectors in η-ϕ space is characterized by the quantity $\Delta R = \sqrt{(\Delta\eta)^2 + (\Delta\phi)^2}$, which is approximately invariant under Lorentz boosts along the z axis.

3 Event Samples

The data samples used in the analysis are recorded using triggers that require the presence of a lepton above a minimum p_{T} threshold, in conjunction with transverse energy associated with jets. The use of multiple trigger requirements is designed to keep individual thresholds relatively low, while maintaining an acceptable trigger rate. During the initial period of the run, the muon data were taken using a single-muon trigger requiring $p_{\mathrm{T}}(\mu) > 8$ GeV and $H_{\mathrm{T}}^{\mathrm{trigger}} > 200$ GeV, where $H_{\mathrm{T}}^{\mathrm{trigger}}$ is the scalar sum of the calorimeter jet [38] p_{T} values satisfying $p_{\mathrm{T}} > 40$ GeV measured at the trigger level. As the LHC luminosity increased, the muon p_{T} threshold was raised to 15 GeV. In the last part of the data-taking period, the $H_{\mathrm{T}}^{\mathrm{trigger}}$ threshold was increased to 250 GeV and the requirement $\not\!\!E_{\mathrm{T}}{}^{\mathrm{trigger}} > 20$ GeV was added, where $\not\!\!E_{\mathrm{T}}{}^{\mathrm{trigger}}$ is the missing transverse energy computed in the High Level Trigger (HLT) using particle-flow algorithms. For electrons, a similar strategy was used. The initial requirements were

$p_T(e) > 10$ GeV and $H_T^{\text{trigger}} > 200$ GeV. Unlike the case for muons, however, a loose isolation requirement was imposed at the trigger level to suppress the rate from electrons in or near jets. The electron p_T threshold was raised to 15 GeV and the H_T^{trigger} requirement to 250 GeV, without any requirement on $\not\!\!E_T$. The offline analysis requirements are designed to be well above the tightest of the trigger configuations, so that the efficiency has reached a plateau.

The analysis procedures are designed by studying simulated event samples based on a variety of generators; in all cases except for certain SUSY scans discussed later, the detector simulation is performed using the GEANT4 package [39]. QCD samples are generated with the PYTHIA 6.4.22 [40] MC generator with tune Z2 [41]. The dominant background, $t\bar{t}$, is studied with a sample generated with MADGRAPH 4.4.12 [42]. The W+jets and Z+jets processes are simulated with both MADGRAPH and ALPGEN [43]. Single-top (s-channel, t-channel, and tW) production is simulated with POWHEG [44]. To assess the effect of multiple pp interactions per beam crossing (pileup), simulated events are reweighted according to the distribution of the number of collision vertices as measured in data.

SUSY benchmark models are generated with PYTHIA. As example CMSSM models, we use LM1, LM3, and LM6 [45]. LM1 is described by the universal scalar mass parameter $m_0 = 60$ GeV, the universal gaugino mass parameter $m_{1/2} = 250$ GeV, the universal trilinear soft SUSY breaking parameter $A_0 = 0$ GeV, the ratio of the two Higgs-doublet vacuum expectation values $\tan\beta = 10$, and the sign of the Higgs mixing parameter $\mu > 0$. LM3 (LM6) is described by $m_0 = 330$ GeV ($m_0 = 85$ GeV), $m_{1/2} = 240$ GeV ($m_{1/2} = 400$) GeV, $A_0 = 0$ GeV ($A_0 = 0$ GeV), $\tan\beta = 20$ (10), and $\mu > 0$. The leading order cross section for these models are 4.9 pb (LM1), 3.4 pb (LM3) and 0.3 pb (LM6); with K factors averaged over the contributing subprocesses, the next-to-leading order cross sections are approximately 6.6 pb (LM1), 4.8 pb (LM3), and 0.4 pb (LM6). For LM1, $m(\tilde{g}) \approx 600$ GeV; the squark masses are in the range 500–600 GeV, except for $m(\tilde{t}) \approx 410$ GeV; and the LSP mass is $m(\tilde{\chi}_1^0) \approx 100$ GeV. In LM3, the masses of the gluino and squarks are very similar (≈ 600 GeV), except for $m(\tilde{t}) \approx 440$ GeV, and the mass of the LSP is $m(\tilde{\chi}_1^0) = 94$ GeV. The LM6 spectrum is heavier, with $m(\tilde{g}) \approx 930$ GeV, $m(\tilde{q}) \approx 800$ GeV, $m(\tilde{t}) \approx 650$ GeV, and $m(\tilde{\chi}_1^0) \approx 160$ GeV. The LM6 cross section is about an order of magnitude smaller than those for LM1 and LM3.

We also perform scans over CMSSM parameter space using a large number of Monte Carlo samples in which the simulation is performed using a CMS fast simulation package to reduce the time associated with the detector simulation.

4 Event Preselection

This section describes preselection requirements, in the context of the overall strategy of the analysis. We also perform an initial survey of the kinematic properties of the event sample to determine whether these are consistent with expectations based on the SM background model.

The offline preselection requirements are designed to be simple and robust. Events are required to have at least one good reconstructed primary vertex, at least three jets, and exactly one isolated muon or exactly one isolated electron. (The detailed jet and lepton selection criteria are specified below.) The lepton-isolation requirement is critical for the rejection of QCD multijet processes, which have very large cross sections. While many lepton candidates are produced in the semileptonic decays of b and c hadrons, from π and K decays in flight, and from misidentification of hadrons, the vast majority of these are embedded in hadronic jets and are rejected using the lepton-isolation variable described below. The initially very large W+jets background (which is dominated by $W \to e\nu$ or $W \to \mu\nu$) is heavily suppressed by the three-jet require-

ment. Depending on the specific selection requirements, either $\bar{t}t$ or W+jets then emerges as the largest contribution to the background in the sample of events with moderate to large values of missing transverse momentum (above approximately 150 GeV).

Because the analysis is part of a broad set of CMS topological SUSY searches involving $\not\!\!E_T$, we veto events containing a second isolated-lepton candidate. This procedure reduces the statistical overlap between the searches in different topologies, provides a clearer phenomenological interpretation of each search, and, in the single-lepton channel, suppresses SM backgrounds that produce two or more isolated leptons. Nevertheless, $\bar{t}t$ backgrounds with dileptons can still feed into the sample, and this contribution must be determined, particularly because the presence of two neutrinos can result in large values of $\not\!\!E_T$. The background involving $W \to \tau\nu$ decays, both from $\bar{t}t$ events and from direct W production, must also be determined.

The primary vertex must satisfy a set of quality requirements, including $|z_{PV}| < 24$ cm and $\rho_{PV} < 2$ cm, where z_{PV} and ρ_{PV} are the longitudinal and transverse distances of the primary vertex with respect to the nominal CMS interaction point.

Jets and $\not\!\!E_T$ are reconstructed using a particle-flow algorithm [46, 47], which combines information from all components of the detector. The $\not\!\!E_T$ vector is defined as the negative of the vector sum of the transverse momenta of all the particles reconstructed and identified by the particle-flow algorithm. (The $\not\!\!E_T$ quantity itself is the magnitude of the $\not\!\!E_T$ vector.) The jet clustering is performed using the anti-k_T clustering algorithm [48] with a distance parameter of 0.5. Corrections based on simulation are applied to the raw jet energies to establish a relative uniform response across the detector in η and an absolute calibrated response in p_T. The performance of CMS jet reconstruction and the corrections are described in Ref. [38]. Jet candidates are required to satisfy quality criteria that suppress noise and spurious energy deposits, and each event must contain at least three jets with $p_T > 40$ GeV and $|\eta| < 2.4$. Jet thresholds are not relevant for the calculation of $\not\!\!E_T$, which is determined from both clustered energy (jets) and unclustered energy observed in the detector.

In the muon channel, the preselection requires a single muon candidate [49] satisfying $p_T(\mu) > 20$ GeV and $|\eta| < 2.1$. Several requirements are imposed on the elements that form the muon candidate. The reconstructed track must have at least 11 hits in the silicon tracker, with an impact parameter d_0 in the transverse plane with respect to the beam spot satisfying $d_0 < 0.02$ cm and an impact parameter d_z with respect to the primary vertex along the z (beam) direction satisfying $|d_z| < 1.0$ cm.

To suppress background in which the muon originates from a semileptonic decay of a b or c quark in a jet, we require that it be spatially isolated from other energy in the event. A cone of size $\Delta R = 0.3$ is constructed around the muon direction in η-ϕ space. The muon combined isolation variable, $I^{comb} = \sum_{\Delta R<0.3}(E_T + p_T)$, is defined as the sum of the transverse energy E_T (as measured in the electromagnetic and hadron calorimeters) and the transverse momentum p_T (as measured in the silicon tracker) of all reconstructed objects within this cone, excluding the muon. This quantity is used to compute the combined isolation relative to the muon transverse momentum, $I^{comb}_{rel} = I^{comb}/p_T(\mu)$, which is required to satisfy $I^{comb}_{rel} < 0.1$. Finally, the muon must satisfy $\Delta R > 0.3$ with respect to all jets with $p_T > 40$ GeV and $|\eta| < 2.4$.

For the electron channel, a single electron candidate [50] is required to satisfy $p_T > 20$ GeV and $|\eta| < 2.4$, excluding the barrel-endcap overlap region (approximately $1.4 < |\eta| < 1.6$). The relative isolation variable, defined as in the muon case, must satisfy $I^{comb}_{rel} < 0.07$ in the barrel region and $I^{comb}_{rel} < 0.06$ in the endcaps, as well as a set of quality and photon-conversion rejection criteria.

Table 1: Main preselection requirements. Additional details are given in the text.

Quantity	Requirement
Jet p_{T} threshold	> 40 GeV
Jet η range	$\lvert\eta\rvert < 2.4$
Number of jets	≥ 3 (LP Variable method),
	≥ 4 (Lepton Spectrum method)
Lepton p_{T} threshold	> 20 GeV
Muon η range	$\lvert\eta\rvert < 2.1$
Muon isolation (relative)	< 0.10
Electron isolation (relative)	< 0.07 (barrel), < 0.06 (endcaps)
Electron η range	$\lvert\eta\rvert < 1.4$, $1.6 < \lvert\eta\rvert < 2.4$
Lepton p_{T} threshold for veto	> 15 GeV

Events with a second lepton are vetoed, for the reasons discussed above. To help suppress the dilepton background, the requirements on the veto leptons are somewhat looser than those on the signal lepton. The p_{T} threshold for both muons and electrons is $p_{\mathrm{T}} > 15$ GeV, and the isolation requirements are looser.

Table 1 summarizes the main variables and requirements used in the event preselection.

Further event-selection requirements are used in the individual background-estimation methods described in Sections 5 and 6. Both methods use the quantity H_{T}, which is defined as the scalar sum of the transverse momenta of jets j with $p_{\mathrm{T}}^{j} > 20$ GeV and $\lvert\eta\rvert < 2.4$,

$$H_{\mathrm{T}} = \sum_{j} p_{\mathrm{T}}^{j}. \tag{1}$$

A simple requirement on the p_{T} of the highest p_{T} or the two highest p_{T} jets can also provide discrimination between signal and background, but such a requirement is more directly sensitive to the mass splittings in a new physics model than H_{T}. Thus, we prefer to use H_{T} to reduce the potential model dependence of the analysis.

Figure 1 shows distributions of H_{T}, $\not\!\!E_{\mathrm{T}}$, and lepton p_{T}. To avoid bias from the trigger selection, we require $H_{\mathrm{T}} > 300$ GeV and $\not\!\!E_{\mathrm{T}} > 60$ GeV in addition to the preselection requirements. The total yield of the simulation was adjusted to match the total yield of events in the data. The dominant backgrounds are $\mathrm{t\bar{t}}$ and W+jets, and the shapes of the observed distributions are well described by the simulation.

5 Lepton Spectrum Method

This section briefly describes the lepton-spectrum method [28, 51] for determining the shape and normalization of the $\not\!\!E_{\mathrm{T}}$ distribution from $\mathrm{t\bar{t}}$ and W+jets backgrounds with a single isolated lepton. These processes account for about 3/4 of the total SM contribution to the signal region, once the loose selection requirements are applied. These requirements consist of the preselection together with $H_{\mathrm{T}} > 500$ GeV and $\not\!\!E_{\mathrm{T}} > 250$ GeV. We define a tight selection by using the same selection as the loose but with $\not\!\!E_{\mathrm{T}} > 350$ GeV.

This section also describes how control samples can be used to measure the non-single-lepton backgrounds, which are significant. These contributions arise mainly from (1) the feed-down of $\mathrm{t\bar{t}}$ dilepton events (≈10%) and (2) either $\mathrm{t\bar{t}}$ or W+jets events with $\tau \to (\mu, \mathrm{e})$ decays (≈15%).

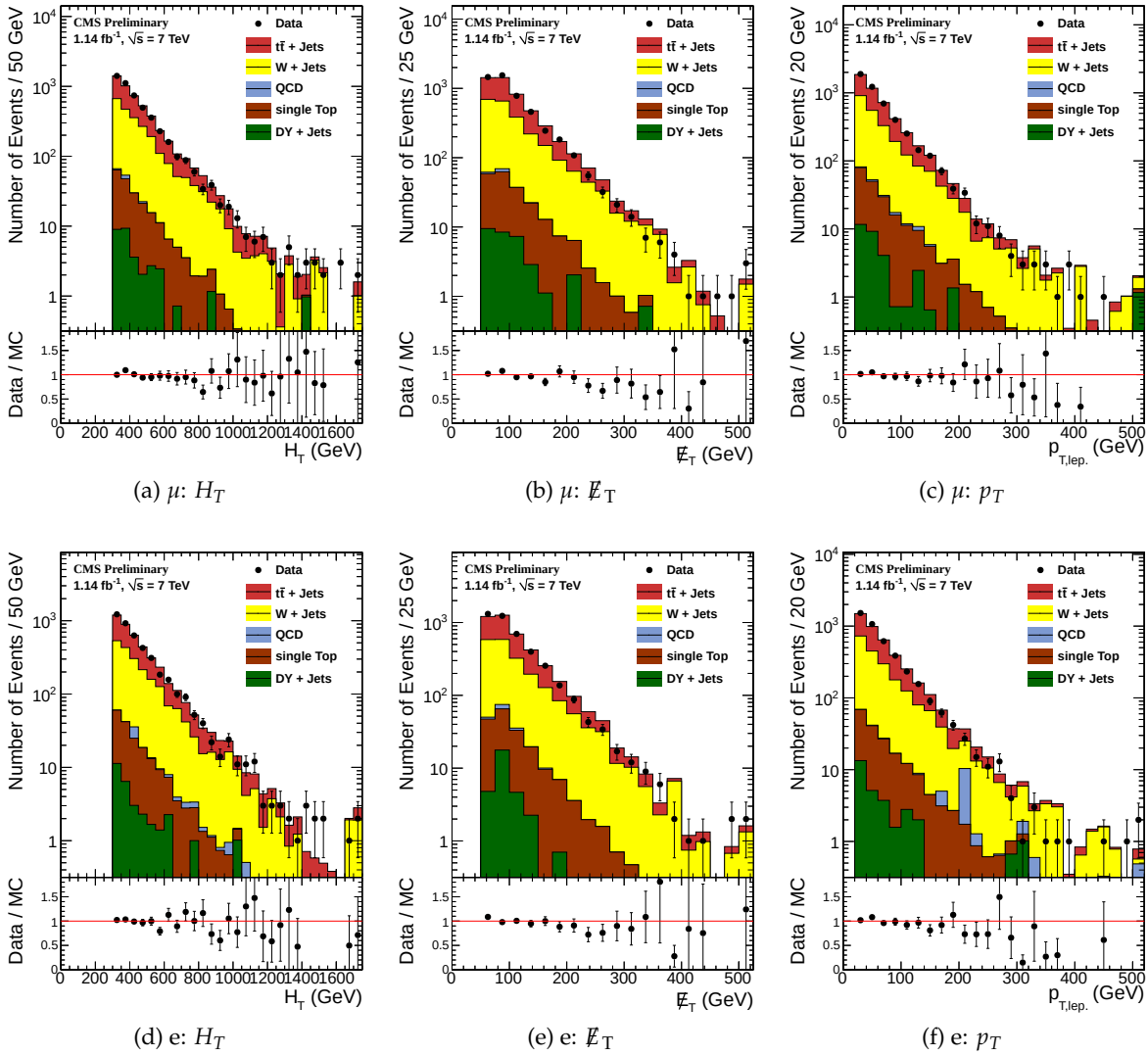

(a) μ: H_T (b) μ: $\not\!\!E_{\mathrm{T}}$ (c) μ: p_T

(d) e: H_T (e) e: $\not\!\!E_{\mathrm{T}}$ (f) e: p_T

Figure 1: Distributions of H_{T} (left), $E_{\mathrm{T}}^{\mathrm{miss}}$ (center) and lepton p_{T} (right) in the muon (a, c, and c) and electron (d, e, and f) channels. The data are shown by the points with error bars, while the stacked histograms show the simulated event samples. The preselection as well as the requirements $H_{\mathrm{T}} > 300$ GeV and $\not\!\!E_{\mathrm{T}} > 60$ GeV have been applied, and the overall yield from simulation is normalized to the data. The yields from the simulated event samples are not the basis for the background predictions in this analysis, which are derived from control samples in the data.

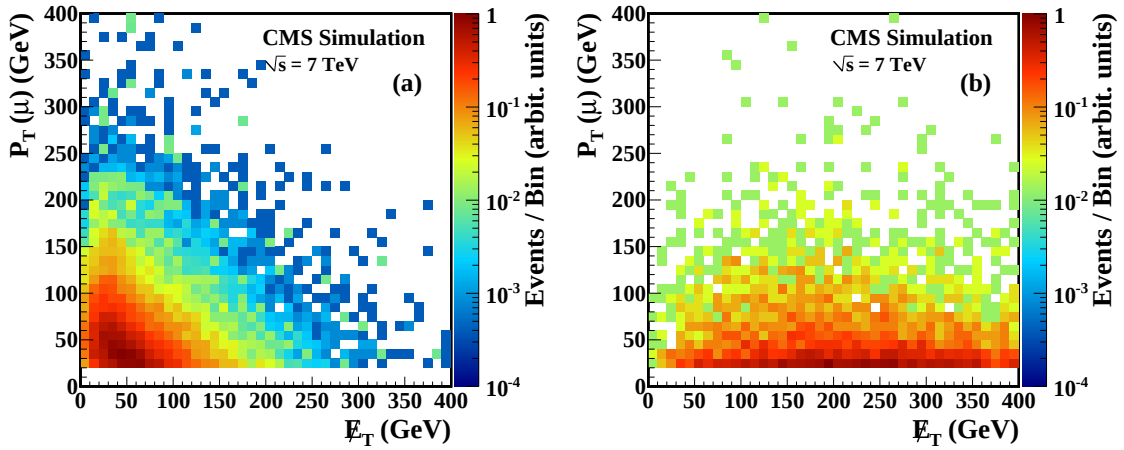

Figure 2: Distributions of muon p_T vs. $\not\!\!E_T$ in the μ channel for (a) simulated $t\bar{t}$ and W+jets events and (b) the LM1 SUSY benchmark model. In $t\bar{t}$ and W+jets events, the lepton p_T and $\not\!\!E_T$ in a given event are anticorrelated, but their distributions are very similar overall. In LM1, which is typical of many SUSY models, the $\not\!\!E_T$ distribution is much harder than the lepton spectrum, since it is dominated by the production of two LSPs.

Although the background from QCD multijet events is very small, we nevertheless measure this component using control samples in the data, because the uncertainties on the simulated QCD event samples are difficult to quantify. We rely on simulated event samples for the determination of two backgrounds, single-top production and Z+jets, whose contributions are estimated to be below one event in total.

The physical foundation of the lepton-spectrum method is that, when the lepton and neutrino are produced together in two-body W decay (either in $t\bar{t}$ or in W+jets events) the lepton spectrum is directly related to the $\not\!\!E_T$ spectrum. With suitable corrections, discussed below, the lepton spectrum can therefore be used to predict the $\not\!\!E_T$ spectrum. In contrast, the $\not\!\!E_T$ distribution in most SUSY models is dominated by the presence of two LSPs. The $\not\!\!E_T$ distribution for such models extends to far higher values than the lepton spectrum. These points are illustrated in Fig. 2, which shows the relationship between lepton-p_T and $\not\!\!E_T$ distributions in the laboratory frame for two simulated event samples: (a) the predicted SM mixture of $t\bar{t}$ and W+jets events and (b) the SUSY LM1 benchmark model. As we will demonstrate, the lepton-spectrum method provides a robust background prediction in the high $\not\!\!E_T$ region, even in the presence of a large SUSY signal, because leptons in SUSY events typically have much lower momenta than the LSPs.

The lepton spectrum is measured with a control sample defined by the preselection and the H_T requirements. Applying a $\not\!\!E_T$ requirement, even a modest one, could bias the high end of the lepton spectrum, which is critical for the measurement. As discussed below, only the muon spectrum is used as a control sample, because the QCD multijet background is significant in the low $\not\!\!E_T$ region of the electron sample.

The overlap between the control sample and the signal region is small: one event for the loose selection and zero events for the tight selection. This can be understood from Fig. 2a. The upper end of the lepton spectrum occurs at low values of $\not\!\!E_T$, which is in the upper left region of the plot. This control sample is used to predict the upper end of the $\not\!\!E_T$ spectrum, which is in the lower right region. Figure 2b shows that most of the leptons from potential SUSY

contamination of the control sample would occur at low lepton p_T and therefore have little effect on the prediction of the background yield in the high $\not\!\!E_T$ region.

To use the lepton spectrum to predict the $\not\!\!E_T$ spectrum in single-lepton SM background processes, three issues must be addressed: (1) the effect of W-boson polarization in both $t\bar{t}$ and W+jets events, (2) the effect of the applied lepton p_T threshold, and (3) the effect of the difference between the experimental resolutions on the measurements of lepton p_T and $\not\!\!E_T$.

We consider the polarization issues first, starting with $t\bar{t}$ production, the largest background. In the decay of a top quark, $t \to bW^+$, the angular distribution of the (positively) charged lepton in the W^+ rest frame can be written

$$\frac{dN}{d\cos\theta_\ell^*} = f_{+1}\frac{3}{8}(1+\cos\theta_\ell^*)^2 + f_{-1}\frac{3}{8}(1-\cos\theta_\ell^*)^2 + f_0\frac{3}{4}\sin^2\theta_\ell^*, \quad (2)$$

where f_{+1}, f_{-1}, and f_0 denote the polarization fractions associated with the W-boson helicities $+1$, -1, and 0, respectively. The angle θ_ℓ^* is the polar angle of the charged lepton in the W^+ rest frame, measured with respect to a z-axis that is collinear with the momentum direction of the W^+ in the top-quark rest frame. (In this expression, the azimuthal angle has been integrated over, removing the interference terms between different helicity amplitudes.) The polarization fractions thus determine the angular distribution of the lepton in the W rest frame and, together with the Lorentz boosts, control the p_T distributions of the lepton and the neutrino in the laboratory frame.

The W polarization fractions in top-quark decay have been calculated [52] with QCD corrections to NNLO, and the polarization is predominantly longitudinal. For $t \to bW^+$ these fractions are $f_0 = 0.687 \pm 0.005$, $f_{-1} = 0.311 \pm 0.005$, and $f_{+1} = 0.0017 \pm 0.0001$. The very small value of f_{+1} is explained by the fact that, since $m_b/m_W \ll 1$, the b quark is highly relativistic and is in a nearly pure helicity $\lambda = -1/2$ state. These precise calculations reduce the uncertainties associated with the W polarization in $t\bar{t}$ events to a low level. The theoretical values are consistent with measurements from the D0 experiment, which obtained [53] $f_0 = 0.669 \pm 0.078 \pm 0.065$ and $f_{+1} = 0.023 \pm 0.041 \pm 0.034$, expressed for the W^+ polarizations.

The W polarization in W+jets events exhibits a more complex behavior than that in $t\bar{t}$ production. CMS has reported first measurements of these effects [36], which are consistent with ALPGEN and MADGRAPH simulations predicting that the W^+ and W^- bosons are both predominantly left-handed in W+jets events at high p_T. An NLO QCD calculation [54] has demonstrated that the predicted polarization fractions are stable with respect to QCD corrections.

The relationship between the lepton p_T spectrum and the $\not\!\!E_T$ distribution is also affected by the threshold ($p_T > 20$ GeV) applied to the leptons. Because of the anticorrelation between the lepton p_T and the $\not\!\!E_T$, the threshold requirement removes SM background events at high $\not\!\!E_T$ but not the events with high-p_T leptons that are used to predict this part of the $\not\!\!E_T$ spectrum. For the $t\bar{t}$ background, this effect partially compensates for the bias from the W polarization. For W+jets events, in contrast, the polarization effects for W^+ and W^- approximately cancel, but the lepton p_T threshold shifts the predicted yield upward. The key point is that the effects of both the polarization and the lepton p_T threshold can be reliably determined.

Finally, the resolution on the reconstructed $\not\!\!E_T$ is poorer than that for the lepton p_T, so the $\not\!\!E_T$ spectrum will be somewhat broadened with respect to the prediction from the lepton spectrum. We measure $\not\!\!E_T$ resolution functions (templates) in the data using QCD multijet events, and use them to smear the measured lepton momenta. The templates are created for events with ≥ 4 jets and are characterized by the H_T range of the events. Because the templates are taken from data, they include not only the intrinsic detector resolutions, but also the effects of cracks and

Table 2: Comparison of SM background yields predicted from control samples in data with expectation based on simulated event samples normalized to the integrated luminosity of the data sample. The yields are given for the defined signal regions (loose selection: $\not\!\!E_T > 250$ GeV and $H_T > 500$ GeV, tight selection: $\not\!\!E_T > 350$ GeV and $H_T > 500$ GeV). The quoted uncertainties are statistical and systematic. For the single-top and Z+jets, only simulated event (MC) samples are used. The QCD prediction from simulated event samples yields zero events for both the loose and the tight selections, but these are denoted as not available (n.a.) because the size of the samples is not sufficiently large to assess this background with a useful precision.

Sample	Loose (e+μ) Control pred.	Loose (e+μ) MC pred.	Tight (e+μ) Control pred.	Tight (e+μ) MC pred.
1 ℓ	$34.6 \pm 7.7 \pm 10.8$	53.6 ± 1.2	$8.8 \pm 3.7 \pm 3.4$	11.9 ± 0.5
Dilepton	$4.0 \pm 3.9 \pm 0.8$	7.6 ± 0.6	$0.9 \pm 1.9 \pm 0.9$	1.4 ± 0.2
1 τ	$10.5 \pm 1.2 \pm 0.5$	12.5 ± 0.6	$2.3 \pm 0.5 \pm 0.2$	3.1 ± 0.3
QCD	$0.0 \pm 1.2 \pm 0.3$	n.a.	$0.0 \pm 1.0 \pm 0.3$	n.a.
1 top,Z+jets	$0.7 \pm 0.2 \pm 0.2$	0.7 ± 0.2	$0.1 \pm 0.1 \pm 0.1$	0.1 ± 0.1
Total SM	$49.8 \pm 8.8 \pm 10.8$	74.4 ± 1.5	$12.1 \pm 4.3 \pm 3.6$	16.5 ± 0.6

acceptance. The overall effect of the smearing is modest, changing the background prediction by 5–15%, depending on the $\not\!\!E_T$ threshold applied.

The raw background predictions based on control samples in data are corrected to account for a specific set of effects. For the single-lepton backgrounds, the effects of the W polarization, the lepton p_T threshold for the signal region, and the $\not\!\!E_T$ energy scale are to produce understood shifts in the $\not\!\!E_T$ spectrum relative to the lepton spectrum. The corrections also account for the small contamination of the single-lepton control sample from dilepton and single-τ events with high p_T leptons. Overall, the lepton p_T spectra from these processes are much softer than the corresponding $\not\!\!E_T$ distributions, and the background predictions must be obtained from separate control samples.

For the loose selection the correction factors for the single-lepton background prediction are 0.85 ± 0.04 for the muon channel and 0.83 ± 0.04 for the electron channel. In the tight selection, the factors are 0.78 ± 0.06 (muons) and 0.74 ± 0.07 (electrons). The uncertainties on the correction factors quoted here are statistical only; systematic uncertainies are discussed below.

Table 2 compares the background yields predicted from the control samples in data with the yields obtained directly from simulation for both the loose and the tight selections. The single-lepton background is the dominant contribution for both the loose and the tight selections. The other background contributions are discussed below. The data-driven predictions are generally somewhat lower than those from simuation.

Figure 3 shows the $\not\!\!E_T$ distribution in data for the combined muon and electron channels, with all of the selection requirements (including $H_T > 500$ GeV), except that on $\not\!\!E_T$ itself. The only difference between the loose and tight selections is the value of the $\not\!\!E_T$ requirement, which is 250 GeV for loose and 350 GeV for tight. The predicted $\not\!\!E_T$ distribution is a sum over three sources: single-lepton backgrounds (from both $t\bar{t}$ and W+jets events), dilepton feed-down from $t\bar{t}$ and single-τ events (from both $t\bar{t}$ and W+jets processes). The $\not\!\!E_T$ distribution from the single-lepton background, which is dominant, is measured from the p_T spectrum of single muon events. The p_T distribution is smeared according an H_T-dependent resolution function taken as a set of templates from QCD multijet events. As discussed above, for a given $\not\!\!E_T$ threshold, a correction factor from simulation is applied to take into account the effect of the lepton p_T

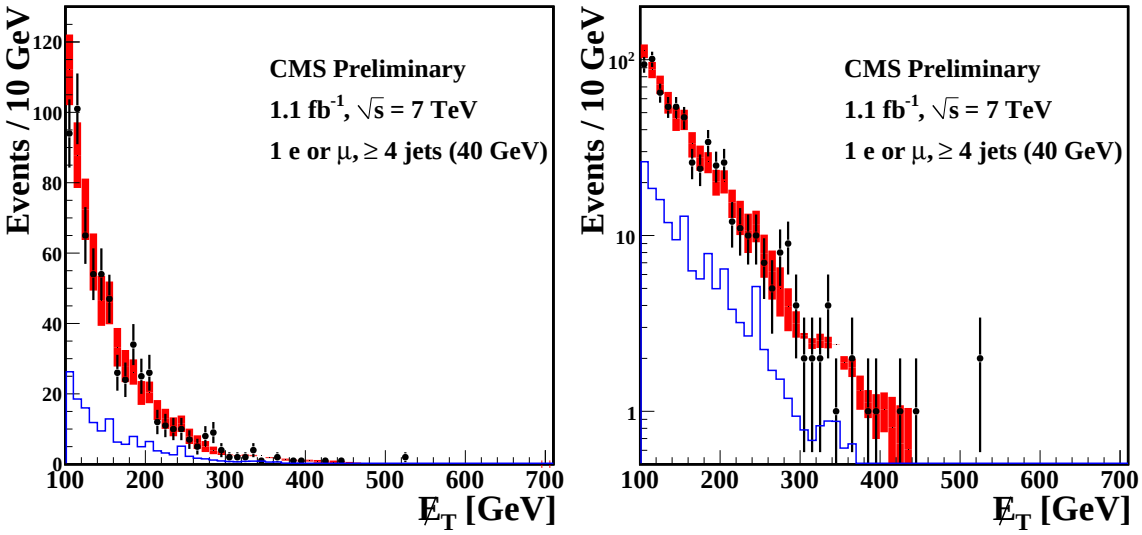

(a) (b)

Figure 3: Distribution of $\not\!\!E_{\mathrm{T}}$ in the data (solid points with error bars) for $H_{\mathrm{T}} > 500$ GeV for the combined muon and electron channels, together with the combined background prediction (red band) from SM single-lepton, dilepton, and $\tau \to \ell$ events, on (a) linear scale and (b) log scale. The contribution from the SM dilepton and $\tau \to \ell$ sources only is shown as a blue histogram.

threshold and polarization effects. For the purposes of illustration, in Fig. 3, a p_{T}-dependent correction factor is applied in each bin of 50 GeV. As a consquence, the background shown above a given threshold in the figure can differ slightly from the value used in the final prediction.

We turn now to the methods used to predict the non-single-lepton backgrounds. These include several categories of dilepton events, events with $\tau \to \ell$ decays (either from $\mathrm{t\bar{t}}$ or W+jets events), and QCD multijet processes. These contributions are also estimated using control samples in the data, as discussed below. The background from single-top production and Drell-Yan/Z+jets is very small for the loose selection and is negligible for the tight selection. These contributions are estimated from Monte Carlo samples and are below one event for both selections.

The dilepton background (including the τ as one of the leptons) can be divided into four contributions: (1) 2ℓ with one ignored lepton, (2) 2ℓ with one lost lepton, (3) $\ell + \tau$ with $\tau \to$ hadrons, and (4) $\ell + \tau$ with $\tau \to$ lepton. An ignored lepton is one that is reconstructed but fails either the lepton identification requirements or the p_{T} threshold requirement. A lost lepton is one that is either not reconstructed or is out of the detector acceptance. Events from processes (1) and (3) account for most of the dilepton background. All of the estimates of the dilepton feed-down backgrounds begin with control samples of reconstructed dilepton events in the ee, eμ, and $\mu\mu$ channels. The $\not\!\!E_{\mathrm{T}}$ distributions in these control samples in data, when suitably modified to reflect the loss of a lepton or the presence of a leptonic or hadronic τ decay, provide an accurate description of the shape of the $\not\!\!E_{\mathrm{T}}$ distribution of the background. Simulated event samples are used to determine, for the four processes described above, the ratio $r_i = N^i_{\mathrm{feed}}/N_{\mathrm{control}}$ of the number of events feeding down to the single-lepton channel to the number of events observed in the control sample, for $\not\!\!E_{\mathrm{T}} < 250$ GeV. This procedure effectively normalizes all such

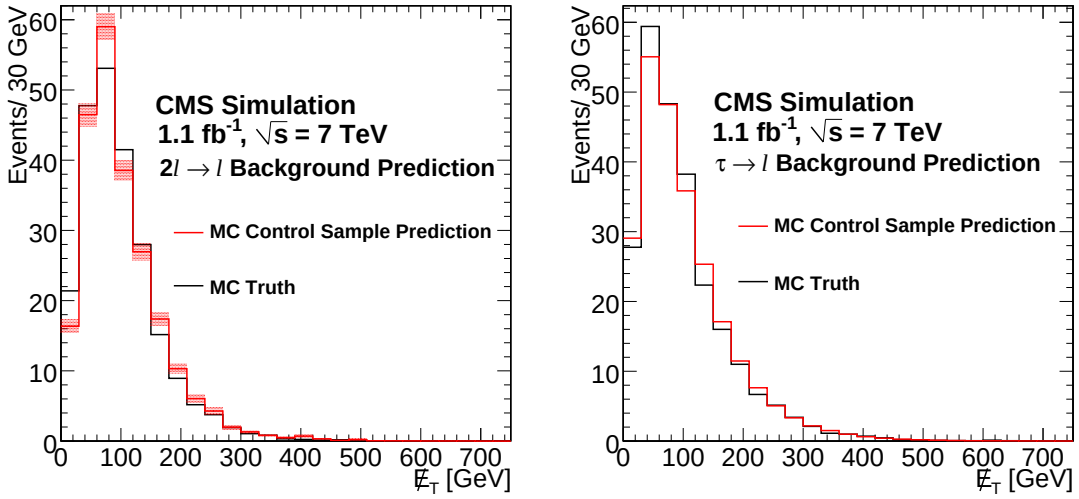

(a) (b)

Figure 4: Tests of the dilepton and τ background prediction methods using simulated (MC) event samples. Each figure compares the $\not\!\!E_{\mathrm{T}}$ distribution after requiring $H_{\mathrm{T}} > 500$ GeV for the true background (black histogram) with that obtained by applying the prediction method to the control samples in the MC (red histogram): (a) dilepton background and (b) $\tau \to \ell$ background.

feed-down contributions to the control samples in data. In all cases, care is required to ensure that the control sample is not contaminated by QCD background. Estimates for the $\tau \to \ell$ single-lepton backgrounds from $\mathrm{t\bar{t}}$ and W+jets processes are based on a similar procedure as that used for the dilepton backgrounds, but in this case the single-lepton sample itself is used as the control sample. We apply correction factors κ_i for each background to compensate for the potential bias of the method at high $\not\!\!E_{\mathrm{T}}$. For the loose selection ($\not\!\!E_{\mathrm{T}} > 250$ GeV and $H_{\mathrm{T}} > 500$ GeV), the correction factors are 0.79 ± 0.22 for the dilepton background and 0.99 ± 0.04 for the $\tau \to \ell$ background. (While these values are consistent with unity, the statistical uncertainty associated with the finite size of the simulated event samples only allows us to conclude that a bias might be present.) The uncertainties on the dilepton and τ background predictions have a statistical component from the number events in the control sample in data and a systematic component related to a number of effects that are assessed with simulated event samples. These include the uncertainty on the ratios r_i and κ_i defined above, the deviation from unity of the ratio of the method's prediction at high $\not\!\!E_{\mathrm{T}}$ to the true value in simulated event samples (i.e., the possible bias of the method in the $\not\!\!E_{\mathrm{T}}$ tail, as measured by $|\kappa_i - 1|$), the statistical uncertainty on this test at high $\not\!\!E_{\mathrm{T}}$, and the effect of propagating the uncertainty on the $\not\!\!E_{\mathrm{T}}$ scale through the prediction algorithm.

Background from QCD multijet events is suppressed to a level well below one event in both the loose and tight selections. To estimate the QCD background, we use the two-dimensional distribution of $\not\!\!E_{\mathrm{T}}$ and the combined relative lepton isolation, $I_{\mathrm{rel}}^{\mathrm{comb}}$ (see Section 4), which are essentially uncorrelated. The details of the method are presented in Ref. [28].

Although very few QCD background events contribute to the signal region at high $\not\!\!E_{\mathrm{T}}$, such events can affect the control region used to estimate the single-lepton background from $\mathrm{t\bar{t}}$ and W+jets events. That control sample is selected without a $\not\!\!E_{\mathrm{T}}$ requirement. In fact, requiring a

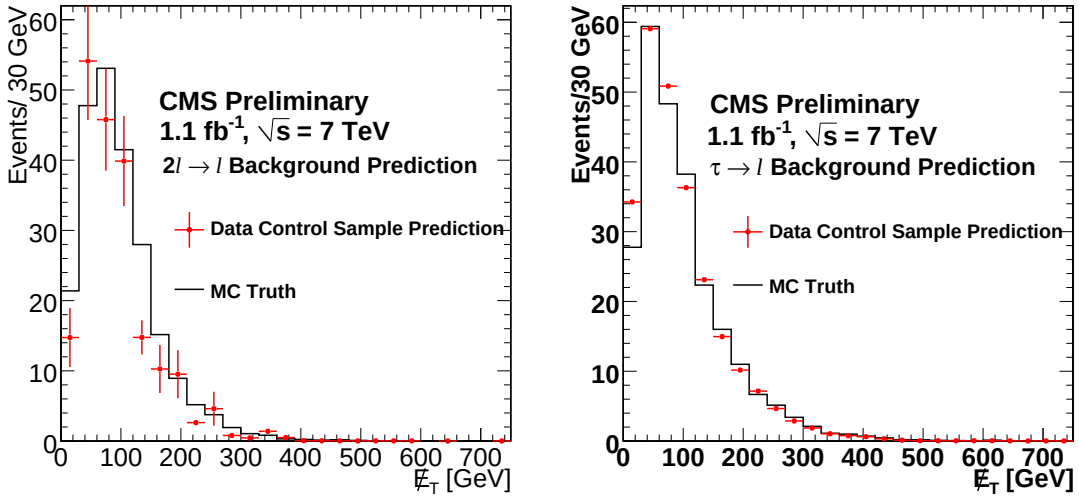

(a) (b)

Figure 5: Predictions for dilepton and $\tau \to \ell$ backgrounds after requiring $H_T > 500$ GeV: control samples in data (red points with error bars) vs. MC predictions (black solid historgram) for (a) Dilepton background and (b) $\tau \to \ell$ background.

minimum value of $\not\!\!E_T$, say $\not\!\!E_T > 25$ GeV, would tend to remove events with high-p_T leptons, which are precisely those used to predict the high-$\not\!\!E_T$ tail. The QCD contamination in the muon sample is very small, but there is significant contamination from QCD in the electron sample at low $\not\!\!E_T$. We have therefore used only the p_T spectrum from the muon control sample to predict the rates for both the electron and muon signal regions. The scaling from the muon to the electron samples is obtained by fitting their ratio in the data over the range $50 < \not\!\!E_T < 150$ GeV, with systematic uncertainties evaluated by varying the fit range. The resulting correction factor, $N(e)/N(\mu) = 0.77 \pm 0.04$, is consistent with the value obtained using simulated event samples. An additional complication is that, as the luminosity increased during the run, the muon trigger rate was controlled by adding a modest $\not\!\!E_T$ requirement ($\not\!\!E_T > 20$ GeV). For this part of the data sample, the shape of the $\not\!\!E_T$ distribution is predicted with a control sample based on muon trigger with the requirements $p_T(\mu) > 30$ GeV and $H_T > 200$ GeV.

Table 3 repeats the predicted SM background yields obtained from control samples in the data and compares these predictions with the observed yields in the signal regions. For the loose selection, $49.8 \pm 8.8 \pm 10.8$ events are predicted compared with 52 events observed. For the tight selection, $12.1 \pm 4.3 \pm 3.6$ events are predicted, compared with 8 events observed. For comparison, the SUSY LM6 benchmark model, which is near the edge of our sensitivity, would contribute 15 events to the signal region for the loose selection and 10 events for the tight selection. In summary, the event yields observed in data are consistent with the SM background predictions listed in Table 3.

The systematic uncertainties on the SM background predictions are included in Tables 2 and 3. The sources of the systematic uncertainties are summarized in Table 4. Details on the evaluation of these uncertainties is given in Ref. [28].

To interpret these results in terms of SUSY models, one also needs signal efficiencies and their associated systematic uncertainties. These quantities, unlike the background predictions, vary across SUSY/CMSSM parameter space, and are discussed in Section 7.

Table 3: Predicted and observed yields in the signal regions for the loose selection ($H_T > 500$ GeV, $\not\!\!E_T > 250$ GeV) and the tight selection ($H_T > 500$, $\not\!\!E_T > 350$ GeV). The quoted uncertainties are statistical and systematic. All background contributions are determined from control samples in the data, except for the single-top and Z-plus-jets contributions, which are obtained from simulated event (MC) samples.

Sample	Loose Selection (e+μ)	Tight Selection (e+μ)
Predicted SM 1 ℓ	$34.6 \pm 7.7 \pm 10.8$	$8.8 \pm 3.7 \pm 3.4$
Predicted SM dilepton	$4.0 \pm 3.9 \pm 0.8$	$0.9 \pm 1.9 \pm 0.9$
Predicted single τ	$10.5 \pm 1.2 \pm 0.5$	$2.3 \pm 0.5 \pm 0.2$
Predicted QCD background	$0.0 \pm 1.2 \pm 0.3$	$0.0 \pm 1.0 \pm 0.3$
Single top (MC), Z+jets (MC)	$0.7 \pm 0.2 \pm 0.2$	$0.1 \pm 0.1 \pm 0.1$
Total predicted SM	$49.8 \pm 8.8 \pm 10.8$	$12.1 \pm 4.3 \pm 3.6$
Data	52	8

Table 4: Summary of systematic uncertainties for the subtraction of the backgound from single-lepton contributions using the lepton-spectrum method. The uncertainty from backgrounds in the control sample is associated primarily with contamination from Z + jets events and, to a lesser extent, from single-top processes.

Source	$\Delta(N_{\text{predicted}}/N_{\text{true}})(\%)$ (Loose selection)	$\Delta(N_{\text{predicted}}/N_{\text{true}})(\%)$ (Tight selection)
$\not\!\!E_T$ and jet energy scale	23	31
W polarization in $t\bar{t}$	4	1.4
W polarization in W+jets	9	15
$\sigma(t\bar{t})$ and $\sigma(W)$	16	16
Lepton efficiency (μ) vs. p_T	4	4
Lepton efficiency (e) vs. p_T	4	4
Backgrounds in control sample	7	7
Total	31	39

6 The Lepton Projection (L_P) Variable Method

The lepton projection method uses the difference in the correlation between the lepton and missing transverse energy, $\not\!\!E_T$, in events which originate from SM processes, namely W+jets and $t\bar{t}$ +jets, from events which originate from sparticle decays. In the former, the helicity of the W boson is accurately predicted in the context of the $V - A$ nature of the W boson coupling to fermions, whereas in the latter no such correlations are expected. Furthermore, in a large part of SUSY parameter space the $\not\!\!E_T$ is largely uncorrelated and larger in magnitude with respect to the lepton.

The CMS collaboration has previously established that W bosons with high transverse momentum, which are produced in association with jets, exhibit a sizable left-handed polarization (see [55]). Therefore, a significant asymmetry in the transverse momentum spectra of the neutrino and charged lepton from subsequent leptonic W decays is expected. Final states with W bosons also arise from t quark ($\bar{t}$) decays, which yield W^+ (W^-) bosons that are predominantly left-handed (right-handed) or longitudinally polarized. The fraction of the helicity states can be determined from an angular analysis of the decay in the center of mass of the W boson. However, the total momentum of the W boson, and therefore its center of mass frame, cannot be accurately determined, since the momentum of the neutrino along the beam axis cannot be

measured. For this reason, we construct an observable, L_P, that depends only on transverse quantities and is still highly correlated to the cosine of the polar angle in the center-of-mass frame [55]:

$$L_P = \frac{\vec{p}_T(\ell) \cdot \vec{p}_T(W)}{|\vec{p}_T(W)|^2}, \tag{3}$$

where $\vec{p}_T(\ell)$ is the transverse momentum of the charged lepton and $\vec{p}_T(W)$ is the transverse momentum of the W boson.

Since SUSY decay chains result in large values of $\not{E}_T$, and often result in relatively low momentum values of the lepton as well, the L_P distribution for SUSY decays tends to peak near zero, whereas W and top decays occupy a broad range of L_P values. In the current analysis two regions are defined: the region with $L_P > 0.3$ is used as the "control region", i.e. a sample which is depleted in the signal expected and is instead dominated by SM processes. The region with $L_P < 0.15$ is used as the "signal region". These values were determined from studies of Monte Carlo samples of W+jets/$t\bar{t}$ and sparticle decays with masses near the region currently under exploration.

The key ingredient of the analysis is the estimate of the number of events in the signal region from SM processes, given the number of events in the control region. A translation factor, R_{CS}, which is the ratio of the number of events in the signal region and control regions for the SM process, is defined:

$$R_{CS} = \frac{N_{MC}(L_P < 0.15)}{N_{MC}(L_P > 0.30)}. \tag{4}$$

The translation factor is obtained from Monte Carlo simulation, and the uncertainties on this factor are included in the sources of systematic uncertainties in the background estimate. Given R_{CS}, the total number of events expected from SM processes in the signal region, $N_{SMpred}(L_P < 0.15)$, can be simply determined from the number of events observed in the data in the control region, $N_{data}(L_P > 0.30)$:

$$N_{SM}^{pred}(L_P < 0.15) = R_{CS} N_{data}(L_P > 0.30). \tag{5}$$

This estimate is then compared to the number of events observed in the data in the signal region, $N_{data}(L_P < 0.15)$ for indications of an excess of events over the SM expectation.

The analysis is performed in different regions of the event "mass scale". To characterize the latter without affecting the correlation of the charged lepton and the neutrino in SM events, the scalar sum of the lepton transverse momentum and the missing transverse energy, S_T^{lep}, is used:

$$S_T^{lep} = p_T(\ell) + \not{E}_T. \tag{6}$$

For W decays, $S_T^{lep} \approx p_T(W)$ at large values of $p_T(W)$. In order to make the search optimization less dependent on the unknown energy scale of a new physics signal, the analysis is performed in disjoint ranges of S_T^{lep} and results in these ranges are combined. In addition, the total transverse energy of the jets considered, H_T, is used.

Table 5: Expected event yields in the signal region, $L_P < 0.15$, with 1.14 fb^{-1} in the muon and electron channels. The MC values are only listed for illustration purposes, since the estimate of the number of SM events in the signal region uses the method described in the text. The contribution from QCD multijet production is expected to be negligible and is thus not included in the table.

$L_P < 0.15$	Muons: S_T^{lep} range (GeV)			Electrons: S_T^{lep} range (GeV)		
Sample	[250-350]	[350-450]	[450-inf]	[250-350]	[350-450]	[450-inf]
$t\bar{t}$ (ℓ)	11.4±0.9	2.91±0.4	0.8±0.2	7.8±0.7	3.0±0.4	1.0±0.3
$t\bar{t}$ ($\ell\ell$)	2.2±0.4	0.6±0.2	0.1±0.1	2.4±0.4	0.7±0.2	0.4±0.2
W	14.5±0.6	8.0±0.5	5.6±0.4	10.5±0.5	5.2±0.4	4.7±0.3
Z	0±1.5	0±1.5	0±1.5	0±1.5	0±1.5	0±1.5
Total MC	28.1±1.1	11.5±0.7	6.5±0.4	20.8±1.0	8.8±0.6	6.1±0.5
LM1	24.2±0.9	23.1±0.9	16.2±0.7	22.9±0.9	20.8±0.8	14.7±0.7
LM3	24.8±0.8	16.7±0.6	9.7±0.5	22.8±0.7	14.8±0.6	9.7±0.5
LM6	1.9±0.0	2.5±0.1	5.9±0.1	1.7±0.0	2.3±0.1	5.3±0.1

The event yields in the muon and electron selections as expected from simulation are shown in Table 5. As discussed previously, the dominant backgrounds to the lepton plus jets and $\not{E}_T$ signature stem from W+jets and $t\bar{t}$ production and decay. Of the two, the production of single W bosons in association with jets, and with large transverse momenta, is in general the larger of the two, especially at lower jet multiplicities. The majority of the $t\bar{t}$ background stems from semi-leptonic $t\bar{t}$ decays, with fully leptonic $t\bar{t}$ decays in which a lepton is either ignored or not reconstructed contributing only a small fraction of events. As indicated in Table 1, the event selection used in this analysis is slightly differerent from the corresponding one in the Lepton-Spectrum analysis. To increase the sensititivity to SUSY decays, this analysis requires three or more jets. While this results in a significant increase in W+jets events, the additional SM background is mostly concentrated in the control region in L_P.

In order to establish that the kinematics of W+jet and $t\bar{t}$ production and decay are well understood, a control sample is defined as all events passing the preselection requirements but confined to low values of S_T^{lep}: $150 < S_T^{lep} < 250$ GeV. The distributions of S_T^{lep}, M_T and the lepton transverse momentum $p_T(\ell)$ in this region are shown in Fig. 7 for the muon channel and in Fig. 6 for the electron channel. In both cases, the Monte Carlo is seen to provide a good description of the data. The corresponding event yields in the data are also found to be in good agreement with the estimate of the total contribution from SM processes. This is described in detail in Sec. 6.3.

In the muon channel, the presence of an inclusive muon trigger allows the usage of an additional control sample. With respect to the preselection, single-muon triggers are used and thus the muon threshold is raised to $p_T(\mu) > 35$ GeV, while the H_T threshold is lowered from 300 GeV to 200 GeV and the jet multiplicity requirement is reversed, requiring less than three jets. Given the lowering of the requirements in H_T and jet multiplicity, this control sample is also dominated by SM processes and therefore this estimate should agree well with the number of events seen in the signal region $L_P < 0.15$. This is illustrated in Table 6 where the event yields in the signal region along with the prediction for the SM expectations are found to be in good agreement.

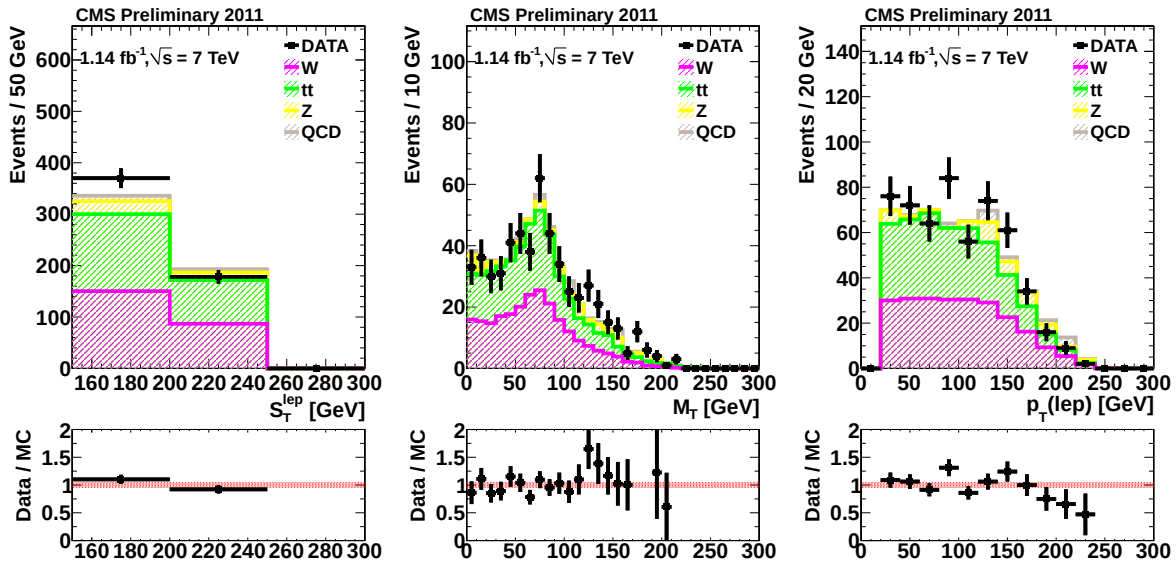

Figure 6: Data and MC comparison for electron events from the preselection and with $S_T^{lep} \in [150 - 250]$ GeV.

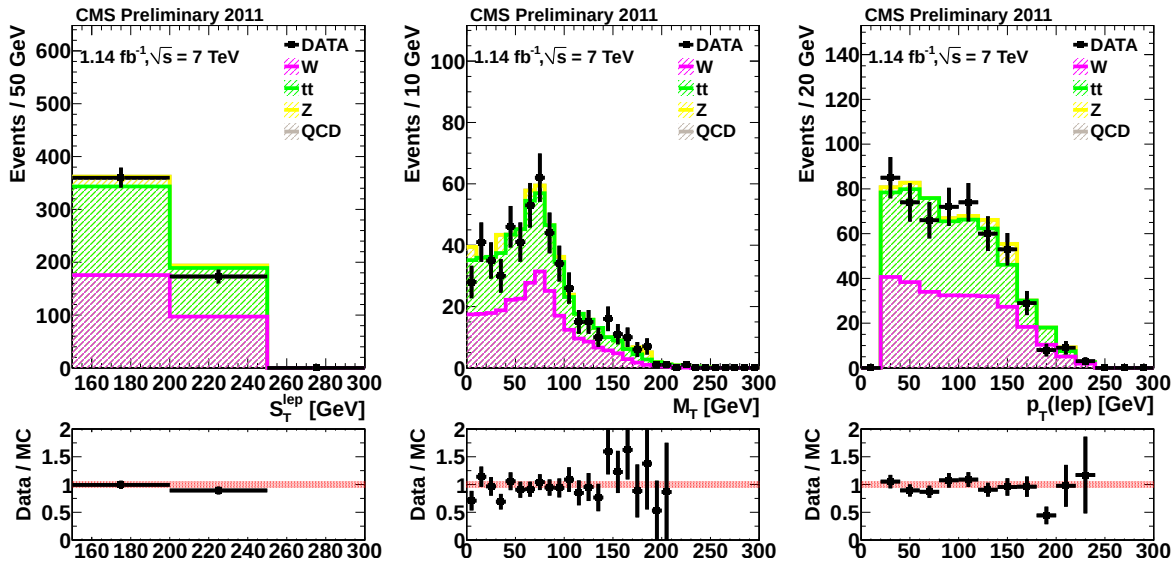

Figure 7: Data and MC comparison for muon events from the preselection and with $S_T^{lep} \in [150 - 250]$ GeV.

6.1 Backgrounds from fake and non-prompt leptons

6.1.1 QCD background in the μ samples

The QCD background in the muon final state is expected to be negligible, and therefore a conservative upper bound is sufficient. As also in the lepton-spectrum analysis, this background is estimated using the relative combined isolation, $I_{\text{comb}}^{\text{rel}}$, where QCD events are expected to populate the region between 0.2 and 0.5. A sample of events enriched in QCD, with $\not{E}_T < 20$ GeV and $\sigma(d_0)/d_0 > 3$, where d_0 is the vertex impact parameter and $\sigma(d_0)$ the uncertainty on it, is employed.

Table 6: Event yields in the muon control sample with < 3 jets and $H_T > 200$ GeV in the signal region, $L_P < 0.15$. The row "SM estimate" is the number of events expected in the signal region, as estimated from the number of events seen in the control region multiplied by the Monte Carlo translation factor R_{CS}. The first uncertainty on the prediction shown is the statistical uncertainty from the control region, the second stems from statistical (limited MC) uncertainty on R_{CS}. The row "data" is the number of events seen in data in the signal region.

$L_P < 0.15$	S_T^{lep} range (GeV)		
Sample	[250-350]	[350-450]	[450-inf]
data	92	24	11
SM estimate	96±10±8	26±6±4	13±4±3
LM6	1.0±0.0	1.0±0.0	2.4±0.1

The relative isolation distributions of QCD events with $\sigma(d_0)/d_0 < 3$ and $\sigma(d_0)/d_0 > 3$ are found to be the same within the statistical unertainties. The ratio $I_{\text{ratio}} = N(I^{\text{rel}}_{\text{comb}} < 0.1)/N(0.2 < I^{\text{rel}}_{\text{comb}} < 0.5)$ is thus measured in this control QCD-enriched sample, and is then used to provide an upper bound for the QCD background in the signal region with the preselection requirements. The ratio obtained is $I_{\text{ratio}} = 8/63$. The remaining EWK contamination in $I^{\text{rel}}_{\text{comb}} < 0.1$ makes this estimate of the QCD fraction conservative. The resulting estimate indicates that the QCD background in the muon channel is negligible.

6.1.2 QCD background in the *e* samples

The main sources of the QCD background in the electron channel are misidentification of hadronic jets and photon conversions. The size of this background is expected to be larger than the corresponding one in the muon samples. Given the limited statistics of the QCD Monte Carlo samples, as well as the larger dependence of this background to details of the simulations, a data-driven method is used to estimate this background.

The method for estimating the QCD background relies on the inversion of one or more of the electron identification requirements, in order to obtain a sample of events dominated by fake electrons. It is found that the inversion of the requirements on the spatial matching of the calorimeter cluster and the charged-particle track in pseudorapidity and azimuth, $\Delta\eta_{in}$ and $\Delta\phi_{in}$ respectively, maintains the relative fraction of the different QCD sources unchanged. To increase the statistics of the anti-selected sample, the requirements on d_0, d_z are removed, whereas the isolation requirement is also relaxed, after confirming that the effect of this relaxation on the L_P shape in the data is negligible. In the Monte Carlo, it is found that the L_P distribution from the anti-selected events describes well the corresponding distribution from QCD background passing all selection requirements.

The QCD shape thus obtained by the electron-ID inversion, is used as a template to fit the full L_P data distribution. In this fit, the EWK template is taken from MC. This approach, which was already applied in the measurement of the W polarization where it is discussed in detail [55], provides a data-driven template for the QCD contamination. The template fit is performed in the control region ($L_P > 0.3$), where the possible presence of signal is highly suppressed. The number of QCD and EWK events obtained by the fit are used to estimate the total SM contamination in the signal region ($L_P < 0.15$).

The fit is performed in bins of S_T^{lep}. The number of QCD and EWK events in the control and signal regions are summarized in Table 10, and is also displayed in Fig. 8. In agreement with

expectations, since low values of L_P favor events with low-p_T leptons and high $\not\!\!E_T$, the QCD contamination in the signal region, $L_P < 0.15$, is found to be negligible.

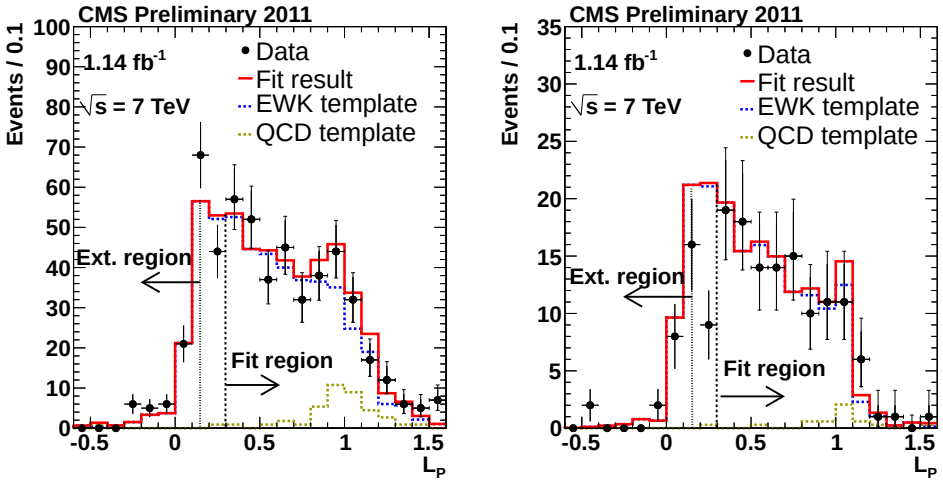

Figure 8: Fit results on data for $S_T^{lep} \in [150-250]$ GeV (left) and $S_T^{lep} \in [250-350]$ GeV (right). The fit is performed in the control region ($L_P > 0.3$) and the result is extrapolated into the signal region ($L_P < 0.15$).

6.2 Systematic uncertainties

The total number of events expected from Standard Model processes in the signal region, $N_{SM}^{pred}(L_P < 0.15)$, is estimated as the product of the translation factor R_{CS} and the number of data events, subtracted for the QCD background, in the control region, $N_{data}(L_P > 0.30)$. There are, therefore, two sources of uncertainty in this estimate: uncertainties in the number of events from EWK processes in the control region and uncertainty in R_{CS}. The procedure for evaluating the systematic uncertainties on both factors is very similar to the one used in the measurement of the W polarization [55]. The sources of systematic uncertainty are:

- Limited statistics of the control region in the data: the limited number of events with $N(L_P > 0.30)$ results in an uncertainty in the SM estimate in the signal region.
- Limited statistics of the MC: the limited statistics of the simulated samples result in a corresponding uncertainty on R_{CS}.
- JES scale uncertainty: each jet in the event, and the remaining hadronic recoil are simultaneously scaled upwards or downwards by 5%. The larger of the two variations is used as the uncertainty.
- Hadronic recoil resolution: the uncertainty on the resolution of the hadronic recoil system was measured in [56], and a difference between the resolution in MC and data of the order of 10% is observed. The resolution is thus increased correspondingly.
- Ratio of $t\bar{t}$/W+jets cross sections: the $t\bar{t}$ and W+jets cross sections are conservatively varied by 30% and 50% respectively. The largest change in R_{CS} is taken as the systematic uncertainty due to this source.
- Muon momentum scale: studies of the Z mass yield a total bias of 1% [57]. To estimate the effect of this bias, the p_T scale is varied according to the followign expression:

$$p'_T = p_T + \text{sign}(\mu) \cdot 0.01 \cdot p_T^2/100 \text{ GeV} \cdot (1 + \sin(\phi))$$

- $t\bar{t}$ and W polarization: the polarization in $t\bar{t}$ events is varied by 5% as in the previous CMS single-lepton analysis. For the polarization in W+jets events the difference in the left-handed and right-handed polarization fractions, $f_L - f_R$, is varied by 15%, consistently with the CMS measurement.
- Fully leptonic $t\bar{t}$: the relative fraction of $t\bar{t}$ events that have more than one lepton (e or μ) and the second lepton is either not reconstructed, or not identified due to the detector acceptance or the veto efficiency, is also considered. Using MC simulation, this background is found to contribute a relatively small fraction of the total SM background, so, a conservative uncertainty of 50% on the number of events is adequate.
- Other sources of systematic uncertainty: the effect of uncertainties in the parton distribution functions (PDF) and in the trigger efficiency are also considered and are found to be negligible.

The relative change in R_{CS} from each source of systematic uncertainty is listed in Table 7 for the muons and in Table 8 for the electrons. The leading uncertainty comes from the limited statistics of the MC. With the current luminosity of 1.1 fb^{-1}, the second largest uncertainty for high S_T^{lep} bins is the statistical uncertainty from the control region. The third biggest uncertainty comes from the Jet Energy Scale, JES. The relative error from the JES scale does not depend strongly on S_T^{lep} and is of relatively moderate size when compared to other analyses involving energetic jets and large $\not{E}_T$. For the electron channel the effect from the JES is larger, since the JES uncertainty also affects the shape of the L_P distrubution used in the fit of the control region.

Table 7: Sources of systematic uncertainty and their effect on the translation factor, R_{CS}, in the muon channel. The relative uncertainty in the estimated number of events in the signal region, stemming from the limited statistics of the control region, is also listed for comparison.

Muons	S_T^{lep} range (GeV)			
Source	[150-250]	[250-350]	[350-450]	> 450
R_{CS}	0.19	0.24	0.26	0.35
$\Delta N/N$ at 1.1 fb^{-1} (%)	13	21	36	41
Systematic uncertainty (%)	15	17	21	34
Control region statistics (%)	5	10	15	24
MC statistics (%)	4	4	8	8
JES uncertainty (Flat 5%) (%)	10	9	8	19
$\not{E}_T$ resolution (10%) (%)	1	3	2	3
Lepton p_T scale (%)	2	2	1	3
W/$t\bar{t}$ ratio (%)	5	5	6	10
$t\bar{t}$ ($\ell\ell$) (%)	5	4	2	1
W polarization (%)	1	1	2	2
$t\bar{t}$ polarization (%)	5	5	5	5

6.3 Result of the L_P analysis

The actual L_P distributions which are used in the search, for different bins in S_T^{lep}, are displayed in Fig. 9 for muons (top) and electrons (bottom).

Table 9 lists the numbers of events observed and the number of events expected from all SM processes as presented above, for the muon channel in the signal region. Similarly, Table 10 lists

Table 8: Sources of systematic uncertainty and their effect on the translation factor, R_{CS}, in the electron channel. The relative uncertainty in the estimated number of events in the signal region, stemming from the limited statistics of the control region, is also listed for comparison.

Electrons	S_T^{lep} range (GeV)			
Source	[150-250]	[250-350]	[350-450]	> 450
R_{CS}	0.16	0.18	0.19	0.23
$\Delta N/N$ at 1.1 fb^{-1} (%)	12	22	38	58
Systematic uncertainty (%)	14	20	24	34
Control region statistics (%)	5	9	17	24
MC statistics (%)	1	10	7	8
JES uncertainty (Flat 5%)(%)	9	10	10	19
$\not{E}_T$ resolution (10%) (%)	2	2	5	7
W/$t\bar{t}$ ratio (%)	6	7	6	10
$t\bar{t}$ ($\ell\ell$) (%)	6	7	6	2
W polarization (%)	1	1	2	3
$t\bar{t}$ polarization (%)	5	5	5	5

Table 9: Event yields in data and MC for the muon search sample with $\geq$ 3 jets and $H_T >$ 500 GeV. The MC yields (in columns "Total MC") are listed for reference only. The background estimate which is used in comparing to the yields in the data is the result of the procedure described earlier and is listed in the column labelled "SM estimate".

	Control Region ($L_P >$0.3)		Signal Region ($L_P <$0.15)		
S_T^{lep} Range (GeV)	Total MC	Data	Total MC	SM estimate	Data
[150-250]	385$\pm$7	368	73.9$\pm$3.0	70.6$\pm$11	84
[250-350]	116$\pm$2	112	28.1$\pm$1.1	27.2$\pm$4.6	29
[350-450]	43.4$\pm$2.	41	11.5$\pm$0.7	10.9$\pm$ 2.3	9
> 450	18.4$\pm$0.8	15	6.5$\pm$0.4	5.3$\pm$ 1.8	6

the corresponding numbers for the elecron channel. The predictions for the muon and electron channels are also displayed graphically in Fig. 10. The errors quoted in Table 10 correspond to the statistical error of the fit, while the error assigned to the prediction in Fig. 10, has also the uncertainty from the potential fluctuation around the prediction included.

All estimates of the total contribution expected from SM processes in the various ranges in S_T^{lep} are in good agreement with the actual numbers of events in the data. There is no visible excess from a potential SUSY signal. The result is interpreted as a limit in SUSY parameter space in the context of the CMMSM in the following section.

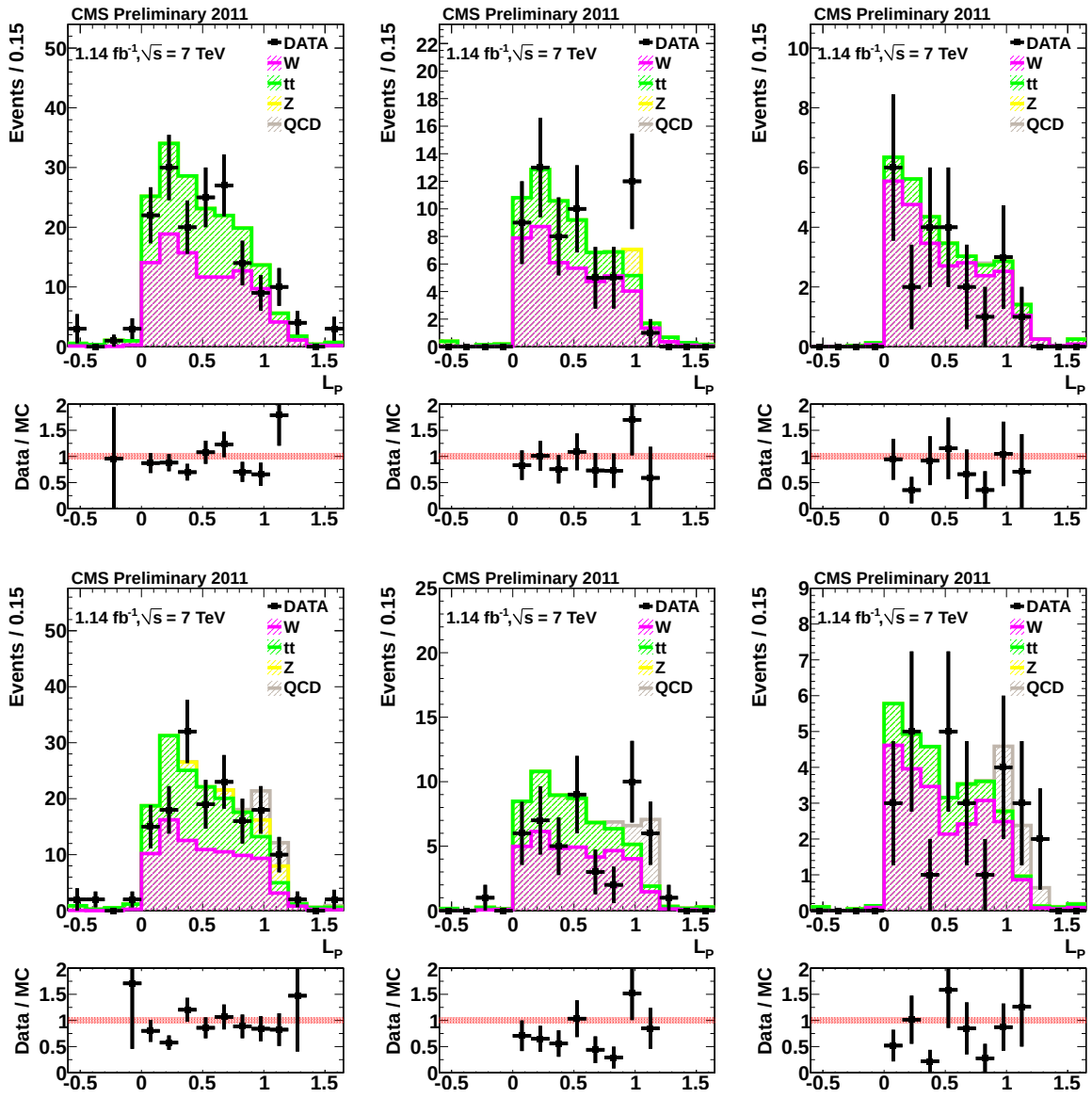

Figure 9: Data and MC comparison of the L_P distribution, for events in the search sample, in different S_T^{lep} regions. Top plots for the muon channel; bottom plots for the electron channel. Left: $S_T^{lep} \in [250 - 350]$ GeV, center: $S_T^{lep} \in [350 - 450]$ GeV, and right: $S_T^{lep} > 450$ GeV.

Table 10: Event yields in data and predictions of the numbers of EWK and QCD events for the electron search sample with $\geq$ 3 jets and $H_T > 500$ GeV. The sum of predicted EWK events and predicted QCD events in the control region is constraint to be equal to the total number of data events. The background estimate which is used in comparing to the yields in the data is the result of the procedure described earlier and is listed in the row labeled "SM estimate". The uncertainty shown for the SM estimate are the full systematic uncertainties. The uncertainties shown for the EWK and QCD contributions are only the statistical uncertainties from the predictions.

	Control Region (L_P >0.3)			Signal Region (L_P <0.15)			
S_T^{lep} Range (GeV)	QCD	EWK	Data	QCD	EWK	SM estimate	Data
[150-250]	39.5±15.5	350±24	390	1.0±0.3	60.8±4.1	61.8±8.7	69
[250-350]	5.0±5.2	117±12	122	0	22.2±2.2	22.2±4.4	21
[350-450]	7.1±3.9	28.9±6.2	36	0	6.9±1.5	6.9±1.7	7
> 450	6.5±5.7	12.5±3.8	19	0	4.3±1.3	4.3±1.5	3

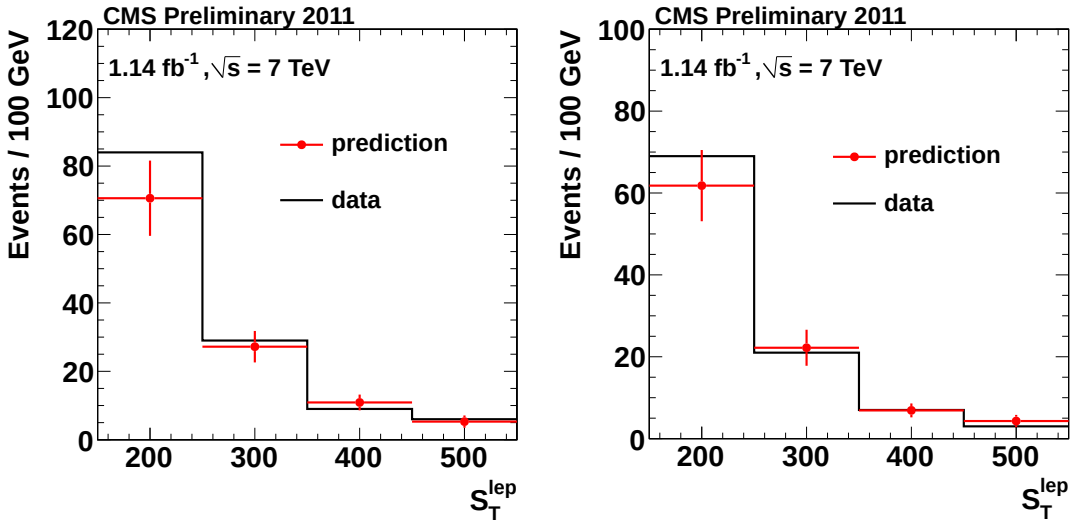

Figure 10: Comparison of the number of events observed in the data and the expectations from the background estimation methods presented above, in the different S_T^{lep} bins. Left: muon channel; Right: Electron channel. The red error-bars indicate the statistical uncertainty of the data only.

7 Results and Interpretation

The Lepton Spectrum and the Lepton Projection methods each yield a SM background prediction that is compatible with the number of events observed in data. In the absence of a signal, we proceed to set exclusion limits on SUSY parameter space. To interpret the absence of a signal in the event sample, scans of CMSSM models are performed to determine whether a given set of parameters is excluded. The Monte Carlo samples are initially generated using leading-order cross sections; the predicted yields are corrected using production-process-dependent NLO cross sections evaluated with PROSPINO [58].

For the Lepton Spectrum method, exclusion plots are obtained for each of the two signal region definitions, loose and tight. The signal efficiency is defined for each model as the number of events passing the reconstructed-event selection, divided by the total number of SUSY events generated in the simulation, summing over all decay chains. (This definition of efficiency therefore incorporates the many different branching fractions leading to single-lepton final states, and it also includes the loss in efficiency associated with the dilepton veto.) The efficiency increases with $m_{1/2}$ but is relatively uniform as a function of m_0.

The systematic uncertainty on the signal efficiency for the Lepton Spectrum method is studied as a function of SUSY parameter space. The uncertainty associated with the scales for the jet energy and $\not\!\!E_{\mathrm{T}}$ is calculated by simultaneouly varying both by $\pm 5\%$. The effect on the efficiency is asymmetric, and for the purpose of limit setting, we take the uncertainty from the decrease in efficiency. This shift is approximately 10% for the loose and tight selections in the SUSY parameter ranges relevant for the limits. The uncertainty associated with the factorization and renormalization scales is evaluated by measuring the change in the signal yield as we vary these scales by 0.5 or 2.0, using process-by-process NLO-to-LO cross section ratios (k-factors) for each simulated signal event. The uncertainty is about 10% for the low m_0 and high m_0 region of the limits; it grows to about 18% in the high m_0 region. Uncertainties of 5% on the lepton selection efficiency and 4.5% on the integrated luminosity are also propagated to the signal yield uncertainty. Although there is some variation in the systematic uncertainties across the $(m_0, m_{1/2})$ plane, we use a constant 20% systematic uncertainty when evaluating the limits. The effect of a variation in the systematic uncertainty from 20% to 15% is smaller than the precision associated with the granularity and statistical flunctuations of the CMSSM scan. The systematic uncertainties on the signal yield and the single-lepton background prediction are modeled as log-normal.

Using the expected signal yield from simulation and the background yield measured from the control samples, we obtain 95% CL upper limits on the cross section for each model point in the SUSY/CMSSW parameter space. A frequentist $\mathrm{CL_s}$ method [59] with a one-sided profile likelihood test statistic is used to obtain the limits. For the purpose of determining the expected limit and $\pm 1\sigma$ bands, the predicted mean number of background events is used for the yield in the signal region.

Fig. 11 shows the limit curves resulting from the loose selection in the lepton spectrum method, evaluated in the $m_{1/2}$ vs. m_0 plane, with the values of the remaining CMSSM parameters fixed at $\tan\beta = 10$, $A_0 = 0$, and $\mu > 0$. The corresponding curves for the tight selection in the lepton spectrum method, which exclude a larger region, are shown in Fig. 12. For reference, the plots include curves of constant gluino and squark masses. The lines of constant gluino mass are approximately horizontal with $m(\tilde{\mathrm{g}}) \approx 2.5\, m_{1/2}$. The lines of constant squark mass are strongly curved in the $m_{1/2}$ vs. m_0 plane. The total signal cross section decreases as a function of $m_{1/2}$ and m_0, roughly following the squark-mass contours.

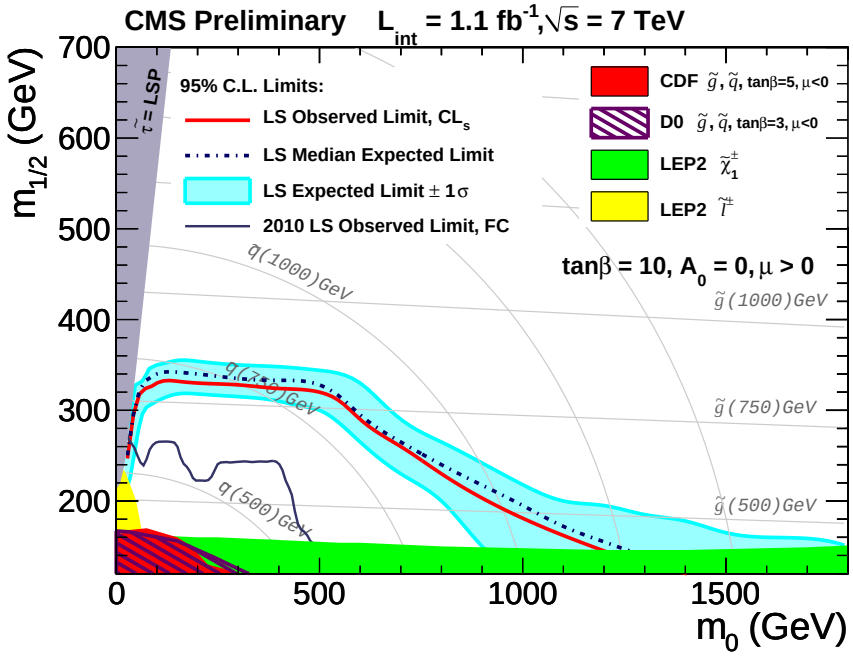

Figure 11: Exclusion region in the CMSSM $m_{1/2}$ vs. m_0 plane for $\tan\beta = 10$, based on the loose selection of the lepton-spectrum method, using the combined electron and muon samples. In addition to the observed limit, the expected limit under the assumption of no signal contribution and the $\pm 1\sigma$ limits are shown.

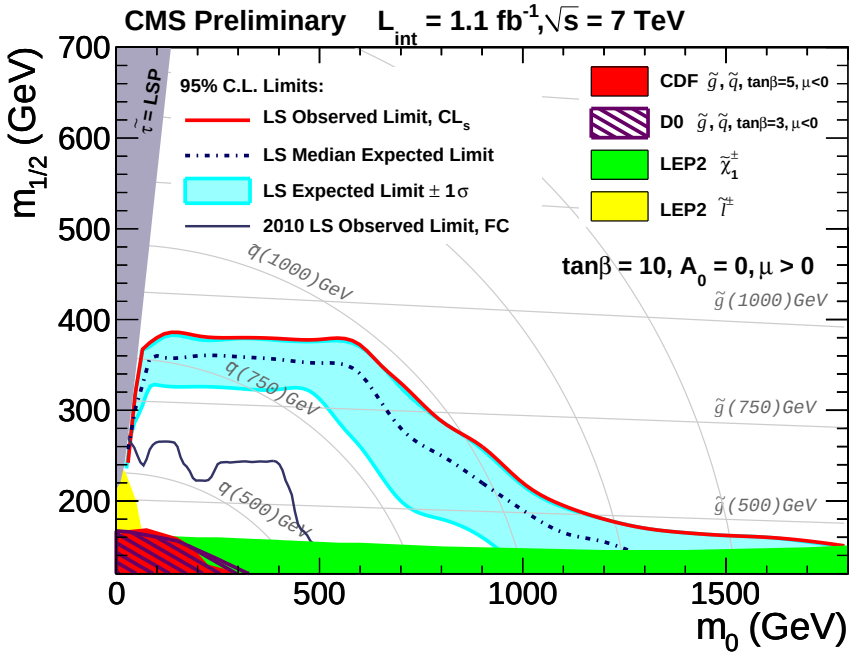

Figure 12: Exclusion region in the CMSSM $m_{1/2}$ vs. m_0 plane for $\tan\beta = 10$, based on the tight selection of the lepton-spectrum method, using the combined electron and muon samples.

Table 11: Summary table of uncertainties related to the signal efficiency for the L_P method.

uncertainty	values
$\mathcal{L}$	4.5%
trigger efficiency	1%
JES 5%	10%-15%, varies between SUSY grid points
$\not{E}_T$ resolution 10%	1%-15%, varies between SUSY grid points
PDF and NLO	10%

For the Lepton Projection method, the limit result is derived by calculating the 95% confidence level upper limit on the MC cross section for the range of the parameters m_0 and $m_{1/2}$. Technically the MC SUSY cross sections are multiplied by a factor f. The maximum value of f is then found for which a particular SUSY parameter point, i.e. a $(m_0, m_{1/2})$ combination, would still be excluded. The CL_s method is used to obtain the limit.

The likelihood to be minimized is schematically given by

$$\mathcal{L}_{\text{STAT}} \times \mathcal{L}_{\text{prior}}$$

where $\mathcal{L}_{\text{STAT}}$ is the statistical component for each S_T^{lep} bin i and $\mathcal{L}_{\text{prior}}$ is the product of all the prior PDFs for the nuisance parameters (Gaussians) as well as the statistical uncertainties which affect the background predictions. The term $\mathcal{L}_{\text{STAT}}$ follows Poisson statistics ($\mathcal{P}$):

$$\mathcal{L}_{\text{STAT}} = \prod_{i \in \text{bins}} \mathcal{P}(n_i^{\text{sig}}(f) + n_i^{\text{bkg}} | N_i^{\text{obs}})$$

where n_i^{bkg} is the data-driven background prediction and $n_i^{\text{sig}}(f)$ the MC signal expectation, and both are functions of parameters in the fit.

The effect on the signal efficiency arising from the uncertainties in the jet energy scale and in the jet resolution is taken into account at each SUSY parameter point. Nuisance parameters for the jet energy scale and resolution uncertainties are included in the signal efficiency as well as the background prediction, thus ensuring that inter-correlations are taken into account. The trigger efficiency is also included as a factor of 0.91 for the muon channel and 0.96 for the electron channel. The uncertainties arising from parton distribution functions and NLO calculations are estimated to be 10% for the full SUSY parameter grid as in the Lepton Spectrum method. The k-factors applied are those produced individually for each grid-point. The integrated luminosity has an uncertainty of 4.5% [60]. A summary of the uncertainties on the signal efficiency can be found in Table 11.

The systematic uncertainties considered for the background prediction are discussed in Sec. 6 and summarized in Tables 7 and 8. In addition, the statistical uncertainty from signal contamination, i.e., the uncertainty arising from the subtraction of an average number of SUSY events from the events in the control region, is considered.

The resulting limit from the L_P method in the $(m_0, m_{1/2})$ plane of the CMSSM for tanβ=10 at NLO is shown in Fig. 13.

Figure 14 shows the constraints from both the Lepton Spectrum method and the Lepton Projection method. The excluded regions are roughly similar. (We do not statistically combine the

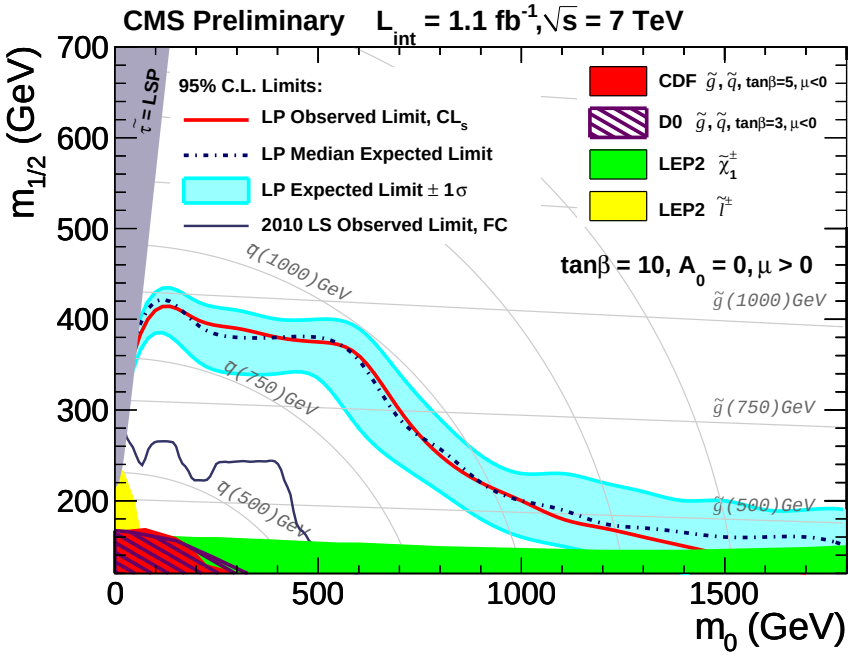

Figure 13: Constraints in the $(m_0, m_{1/2})$ plane for tanβ=10 from the Lepton Projection (L_P) Variable method. The curves show the observed limit and the expected limit with the associated $\pm 1\sigma$ band.

result of the two methods because of the complicated statistical correlations.) In the CMSSM, the gluino mass is $m(\tilde{g}) \approx 2.5 m_{1/2}$. For the region $m_0 < 500$ GeV, one can therefore conclude that gluino masses below about 900 GeV are excluded.

8 Conclusions

Using a sample of proton-proton collisions at $\sqrt{s} = 7$ TeV corresponding to an integrated luminosity of 1.1 fb^{-1}, we have performed a search for new physics with the experimental signature of at least three jets, an isolated, high-p_T lepton, and large missing transverse momentum. The overall shapes of the kinematic distributions observed in data are consistent with expectations from SM simulated event samples, indicating that the sample is dominated by $t\bar{t}$ and W+jets events.

The *Lepton Spectrum* method relies on the close relationship between two fundamental observables: the lepton p_T distribution and the $\not\!\!E_T$ distribution, in the dominant SM background backgrounds with a single isolated lepton. This connection arises from the fact that the lepton and neutrino are produced together in the two-body decay of the W boson, for both $t\bar{t}$ and W+jets events. Smaller backgrounds from the feed-down of $t\bar{t}$ dilepton events, from $\tau \to \ell$ decays in $t\bar{t}$ or W+jets events, and from QCD multijet processes are also estimated from control samples in the data. In the sample investigated with this method, at least four jets are required, which helps to suppress W+jets background. Two signal regions are considered, characterized by different thresholds on $\not\!\!E_T$. The observed yields in each region are consistent with the background estimates based on control samples in the data.

The *Lepton Projection (L_P)* method exploits information on the W-boson polarization in $t\bar{t}$ and W+jets events. The L_P variable encodes information on both the angular distribution of the

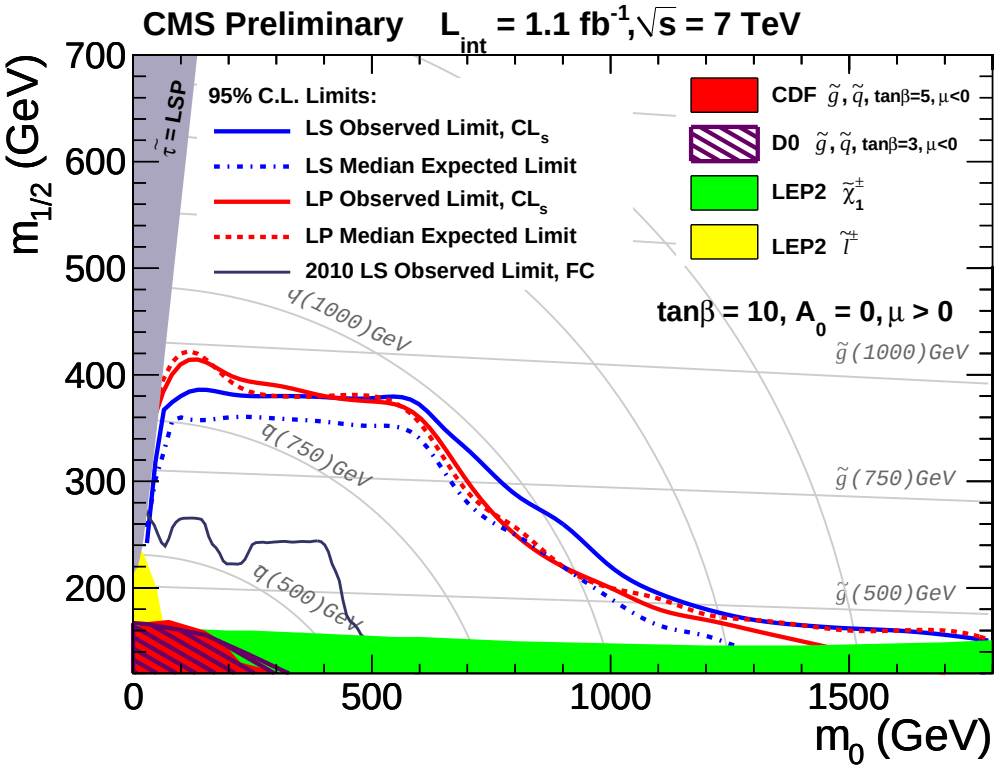

Figure 14: Exclusion region in the CMSSM $m_{1/2}$ vs. m_0 plane for $\tan\beta = 10$, shown for both the Lepton Spectrum method (LS) with the tight selection and the Lepton Projection Variable method (LP).

lepton relative to the lepton + $\not{E}_T$ system, as well as the relative size of lepton p_T and $\not{E}_T$. The L_P method is used to probe the sample of eventes with ≥ 3 jets. The yields observed in the defined signal regions are, as with the Lepton Spectrum a pproach, consistent with the estimate of the total expectation from SM processes.

In the absence of any significant excess of observed events in the data, we interpret these results in the framework of the CMSSM, reporting exclusion regions as a function of $m_{1/2}$ and m_0, for $\tan\beta = 10$. The results exclude gluino masses below ≈900 GeV for m_0 below ≈500 GeV in the context of the CMSSM framework.

References

[1] F. Zwicky, "Die Rotverschiebung von extragalaktischen Nebeln", *Helv. Physica Acta* **6** (1933) 110.

[2] V. Trimble, "The Existence and Nature of Dark Matter in the Universe", *Ann. Rev. Astron. Astrophys.* **25** (1987) 425. doi:10.1146/annurev.aa.25.090187.002233.

[3] M. Bartelmann, "The Dark Universe", *Rev. Mod. Phys.* **82** (2010) 1. doi:10.1103/RevModPhys.82.331.

[4] J. Feng, "Dark Matter Candidates from Particle Physics and Methods of Detection", *Ann. Rev. Astron. Astrophys.* **48** (2010) 495. doi:10.1146/annurev-astro-082708-101659.

[5] E. Witten, "Dynamical Breaking of Supersymmetry", *Nucl. Phys. B* **188** (1981) 513. doi:10.1016/0550-3213(81)90006-7.

[6] S. Dimopoulos and H. Georgi, "Softly Broken Supersymmetry and SU(5)", *Nucl. Phys. B* **193** (1981) 150. doi:10.1016/0550-3213(81)90522-8.

[7] CMS Collaboration, "Absolute Calibration of Luminosity Measurement at CMS: SUmmer 2011 Update", CMS Detector Performance Summary CMS-PAS-EWK-11-001, (2011).

[8] J. Martin, "A Supersymmetry Primer", (1997). arXiv:9709356.

[9] J. Wess and B. Zumino, "Supergauge transformations in four dimensions", *Nucl. Phys. B* **70** (1974) 39. doi:10.1016/0550-3213(74)90355-1.

[10] H. P. Nilles, "Supersymmetry, Supergravity and Particle Physics", *Phys. Reports* **110** (1984) 1. doi:10.1016/0370-1573(84)90008-5.

[11] H. E. Haber and G. L. Kane, "The Search for Supersymmetry: Probing Physics Beyond the Standard Model", *Phys. Reports* **117** (1987) 75. doi:doi:10.1016/0370-1573(85)90051-1.

[12] R. Barbieri, S. Ferrara, and C. A. Savoy, "Gauge Models with Spontaneously Broken Local Supersymmetry", *Phys. Lett. B* **119** (1982) 343. doi:10.1016/0370-2693(82)90685-2.

[13] S. Dawson, E. Eichten, and C. Quigg, "Search for Supersymmetric Particles in Hadron - Hadron Collisions", *Phys. Rev. D* **31** (1985) 1581. doi:10.1103/PhysRevD.31.1581.

[14] CDF Collaboration, "Inclusive Search for Squark and Gluino Production in $p\bar{p}$ Collisions at $\sqrt{s} = 1.96$ TeV", *Phys. Rev. Lett.* **102** (2009) 121801. doi:10.1103/PhysRevLett.102.121801.

[15] D0 Collaboration, "Search for squarks and gluinos in events with jets and missing transverse energy using 2.1 fb^{-1} of p$\bar{\text{p}}$ collision data at $\sqrt{s} = 1.96$ TeV", *Phys. Lett. B* **660** (2008) 449. doi:10.1016/j.physletb.2008.01.042.

[16] D0 Collaboration, "Search for associated production of charginos and neutralinos in the trilepton final state using 2.3 fb^{-1} of data", *Phys. Lett. B* **680** (2009) 34. doi:10.1016/j.physletb.2009.08.011.

[17] Joint SUSY Working Group (ALEPH, DELPHI, L3 and OPAL) Collaboration, "Interpretation of the results in Minimal SUGRA", (2002). LEPSUSYWG/02-06.2.

[18] ALEPH Collaboration, "Absolute mass lower limit for the lightest neutralino of the MSSM from e^+e^- data at $\sqrt{s}$ up to 209 GeV", *Phys. Lett. B* **583** (2004) 247. See also references therein. doi:10.1016/j.physletb.2003.12.066.

[19] DELPHI Collaboration, "Searches for supersymmetric particles in e^+e^- collisions up to 208 GeV and interpretation of the results within the MSSM", *Eur. Phys. J. C* **31** (2003) 421. See also references therein. doi:10.1140/epjc/s2003-01355-5.

[20] L3 Collaboration, "Search for scalar leptons and scalar quarks at LEP", *Phys. Lett. B* **580** (2004) 37. See also references therein. doi:10.1016/j.physletb.2003.10.010.

[21] OPAL Collaboration, "Search for chargino and neutralino production at $\sqrt{s} = 192 - 209$ GeV at LEP", *Eur. Phys. J. C* **35** (2004) 1. See also references therein. doi:10.1140/epjc/s2004-01758-8.

[22] CMS Collaboration, "Search for Supersymmetry in pp Collisions at 7 TeV in Events with Jets and Missing Transverse Energy", *Phys. Lett. B* **698** (2011) 196. doi:10.1016/j.physletb.2011.03.021.

[23] CMS Collaboration, "Search for Supersymmetry in pp Collisions at $\sqrt{s}$ = 7 TeV in Events with Two Photons and Missing Transverse Energy", (2011). arXiv:1103.0953. Submitted to Physical Review Letters.

[24] CMS Collaboration, "Search for new physics with same-sign isolated dilepton events with jets and missing transverse energy at the LHC", (2011). arXiv:1104.3168. Submitted to JHEP.

[25] CMS Collaboration, "Search for Physics Beyond the Standard Model in Opposite-sign Dilepton Events in pp Collisions at $\sqrt{s}$ = 7 TeV", (2011). arXiv:1103.1348. Submitted to JHEP.

[26] CMS Collaboration, "Search for supersymmetry in events with a lepton, a photon, and large missing transverse energy in pp collisions at $\sqrt{s}$ = 7 TeV", (2011). arXiv:1105.3152. Submitted to JHEP.

[27] CMS Collaboration, "Search for Physics Beyond the Standard Model Using Multilepton Signatures in pp Collisions at sqrt(s)=7 TeV", (2011). arXiv:1106.0933. Submitted to PLB.

[28] CMS Collaboration, "Search for supersymmetry in pp collisions at $\sqrt{s} = 7$ TeV in events with a single lepton, jets, and missing transverse momentum", (2011). arXiv:1107.1870. Submitted to JHEP.

[29] ATLAS Collaboration, "Search for supersymmetry using final states with one lepton, jets, and missing transverse momentum with the ATLAS detector in $\sqrt{s} = 7$ TeV pp collisions", *Phys. Rev. Lett.* **106** (2011) 131802. doi:10.1103/PhysRevLett.106.131802.

[30] ATLAS Collaboration, "Search for squarks and gluinos using final states with jets and missing transverse momentum with the ATLAS detector in $\sqrt{s} = 7$ TeV proton-proton collisions", *Phys. Lett. B* **701** (2011) 186. doi:10.1016/j.physletb.2011.05.061.

[31] ATLAS Collaboration, "Search for supersymmetry in pp collisions at $\sqrt{s} = 7$ TeV in final states with missing transverse momentum and b-jets", (2011). arXiv:1103.4344.

[32] ATLAS Collaboration, "Search for supersymmetric particles in events with lepton pairs and large missing transverse momentum in $\sqrt{s} = 7$ TeV proton-proton collisions at the ATLAS experiment", (2011). arXiv:1103.6214.

[33] ATLAS Collaboration, "Search for an excess of events with an identical flavour lepton pair and significant missing transverse momentum in $\sqrt{s} = 7$ TeV proton-proton collisions with the ATLAS detector", (2011). arXiv:1103.6208.

[34] G. L. Kane, C. F. Kolda, L. Roszkowski et al., "Study of constrained minimal supersymmetry", *Phys. Rev. D* **49** (1994) 6173. doi:10.1103/PhysRevD.49.6173.

[35] A. H. Chamseddine, R. Arnowitt, and P. Nath, "Locally Supersymmetric Grand Unification", *Phys. Rev. Lett.* **49** (1982) 970. doi:10.1103/PhysRevLett.49.970.

[36] CMS Collaboration, "Measurement of the Polarization of W Bosons with Large Transverse Momentum in W+Jets Events at the LHC", *Phys. Rev. Lett.* **107** (2011) 021802. doi:10.1103/PhysRevLett.107.021802.

[37] CMS Collaboration, "The CMS experiment at the CERN LHC", *JINST* **0803** (2008) S08004. doi:10.1088/1748-0221/3/08/S08004.

[38] CMS Collaboration, "Determination of Jet Energy Calibration and Transverse Momentum Resolution in CMS", (2011). arXiv:1107.4277. Submitted to JINST.

[39] GEANT4 Collaboration, "GEANT4: A simulation toolkit", *Nucl. Instrum. Meth. A* **506** (2003) 250. doi:10.1016/S0168-9002(03)01368-8.

[40] T. Sjöstrand, S. Mrenna, and P. Z. Skands, "PYTHIA 6.4 Physics and Manual; v6.420, tune D6T", *JHEP* **05** (2006) 026. doi:10.1088/1126-6708/2006/05/026.

[41] R. Field, "Early LHC underlying event data - findings and surprises", (2010). arXiv:1010.3558.

[42] J. Alwall et al., "MadGraph/MadEvent v4: The New Web Generation", *JHEP* **09** (2007) 028. doi:10.1088/1126-6708/2007/09/028.

[43] M.L. Mangano, M. Moretti, F. Piccinini, R. Pittau and A. Polosa, "ALPGEN, a generator for hard multiparton processes in hadronic collisions", *JHEP* **07** (2003) 001. doi:10.1088/1126-6708/2003/07/001.

[44] S. Frixione, P. Nason, and C. Oleari, "Matching NLO QCD computations with parton shower simulations: the POWHEG method", *JHEP* **11** (2007) 070, arXiv:0709.2092. doi:10.1088/1126-6708/2007/11/070.

[45] CMS Collaboration, "CMS technical design report, volume II: Physics performance", *J. Phys. G* **34** (2007) 995. doi:10.1088/0954-3899/34/6/S01.

[46] CMS Collaboration, "Particle–Flow Event Reconstruction in CMS and Performance for Jets, Taus, and $E_{\mathrm{T}}^{\mathrm{miss}}$", CMS Physics Analysis Summary CMS-PAS-PFT-09-001, (2009).

[47] CMS Collaboration, "Commissioning of the Particle-Flow Reconstruction in Minimum-Bias and Jet Events from pp Collisions at 7 TeV", CMS Physics Analysis Summary CMS-PAS-PFT-10-002, (2010).

[48] M. Cacciari, G. P. Salam, and G. Soyez, "The anti-k_{T} jet clustering algorithm", *JHEP* **0804** (2008) 063. doi:10.1088/1126-6708/2008/04/063.

[49] CMS Collaboration, "Performance of muon identification in pp collisions at $\sqrt{s}$ = 7 TeV", CMS Physics Analysis Summary CMS-PAS-MUO-10-002, (2010).

[50] CMS Collaboration, "Electron Reconstruction and Identification at $\sqrt{s} = 7$ TeV", CMS Physics Analysis Summary CMS-PAS-EGM-10-004, (2010).

[51] V. Pavlunin, "Modeling missing transverse energy in V+jets at the CERN LHC", (2009). arXiv:0906.5016.

[52] A. Czarnecki, J. Korner, and J. Piclum, "Helicity fractions of W bosons from top quark decays at next-to-next-to leading order in QCD", *Phys. Rev. D* **81** (2010) 111503(R). doi:10.1103/PhysRevD.81.111503.

[53] D0 Collaboration, "Measurement of the W boson helicity in top quark decyas using 5.4 fb^{-1} of $p\bar{p}$ collision data", *Phys. Rev. D.* **83** (2011) 032009. doi:10.1103/PhysRevD.83.032009.

[54] Z. Bern et al., "Left-handed W bosons at the LHC", (2011). arXiv:1103.5445.

[55] CMS collaboration, "Measurement of the Polarization of W Bosons with Large Transverse Momenta in W+Jets Events at the LHC", *Phys. Rev. Lett.* **107** (2011) 021802. doi:10.1103/PhysRevLett.107.021802.

[56] CMS Collaboration, "Missing transverse energy performance of the CMS detector", (2011). arXiv:1106.5048. Submitted to JINST.

[57] CMS Collaboration, "Performance of muon identification in 2010 data", *CMS Physics Analysis Summary* **CMS-PAS-MUO-10-004** (2011).

[58] W. Beenakker, R. Hopker, M. Spira et al., "Squark and gluino production at hadron colliders", *Nucl. Phys. B* **492** (1997) 51. doi:10.1016/S0550-3213(97)00084-9.

[59] Particle Data Group Collaboration, "Review of particle physics", *J. Phys.* **G 37** (2010) 075021. doi:10.1088/0954-3899/37/7A/075021.

[60] CMS Collaboration, "Absolute Calibration of Luminosity Measurement at CMS: Summer 2011 Update", *CMS Physics Analysis Summary* **CMS-PAS-EWK-11-001** (2011).